Platinum-group elements in the UG1 and UG2 chromitites, and the Bastard reef, at Impala platinum mine, western Bushveld Complex, South Africa: Evidence for late magmatic cumulate instability and reef constitution

Wolf Maier
Centre for Exploration Targeting, University of Western Australia, Crawley 6009, Australia.
e-mail: wdmaier@cyllene.uwa.edu.au

Sarah-Jane Barnes
Sciences de la Terre, Université du Québec à Chicoutimi, Chicoutimi G7H 2B1, Canada.
e-mail: sjbarnes@uqac.ca

ABSTRACT

We have examined the UG1 and UG2 chromitites, the Bastard Reef, and ultramafic rocks in the footwall of the Merensky Reef that are possibly correlatives to the Pseudoreef, in drill core at Impala platinum mine. The UG2 consists of a 66 cm main seam and, ca 5 m above the UG2, four subsidiary seams with a combined thickness of 30 cm. The UG1 consists of a 112 cm main seam and, in its hanging- and foot wall, 50 subsidiary seams/stringers with a combined thickness of 91 cm. The UG2 main seam contains 2111 ppb Pt, 1214 ppb Pd, 362 ppb Ru, and 98 ppb Ir, with the subsidiary seams containing broadly similar PGE levels. The UG1 main seam contains 628 ppb Pt, 265 ppb Ru, and 45 ppb Ir over 112 cm, but only 13 ppb Pd. The subsidiary seams have variable compositions broadly overlapping with the main seam. Well defined positive correlations between Pt and Pd with the IPGE suggest that in the chromitites the PGE were originally concentrated by a sulfide liquid. In both the UG2 and the UG1 chromitites the highest PGE contents occur at the top and bottom of the seams, analogous to other localities in the Bushveld Complex. Such element distribution patterns resemble those in certain dykes interpreted to result from flow differentiation, suggesting that the seams formed via injection of chromite slurries into their semi- consolidated footwall cumulates, possibly during sagging of the centre of the complex in response to emptying of staging chambers at depth. Down-dip sliding of the semi-consolidated cumulates was also responsible for the phase layering of the chromitites, as represented by the sharp top and bottom contacts of the seams, and the extremely well defined correlation between PGE and chromitites. One of the last processes during cumulate solidification involved removal of some of the sulfur from the chromitites by late magmatic and/or hydrothermal fluids. Pd and Cu have also been mobilized locally (particularly in the UG1 chromitite), but the other PGE appear to have been largely immobile.

Introduction

The origin of the PGE mineralization in the chromitites of the Bushveld Complex and other layered intrusions remains unresolved. The chromitites tend to be highly PGE enriched relative to the associated silicate rocks, but contain few sulfides (mostly <100 ppm S). A model of collection of the PGE by magmatic sulfides, as accepted for many PGE deposits elsewhere, is thus not obvious yet the nature of alternative phases that may have concentrated the PGE remains unclear. Several authors (*e.g.* Gain 1985, Maier 2005) have suggested that the scarcity of sulfides may be due to resorption of sulfide during magma ascent or cumulate solidification, but such models are difficult to evaluate because only few detailed compositional studies of chromitite seams have been published. The present study aims to provide added constraints by presenting a detailed documentation of the concentrations of the PGE and some lithophile elements through the UG2 and UG1 chromitites and their foot- and hanging walls on the farm Reinkoyalskraal 278JQ, Impala platinum mines, western Bushveld Complex (Figure 1). In order to be able to place the chromitites into a broader stratigraphic context, we also examined, on the adjacent farm Vlakfontein, a section through the Bastard Reef and several samples of ultramafic rocks in the footwall of the Merensky Reef that could represent correlatives of the Pseudoreefs (Maier and Eales, 1997).

Previous work

Stratigraphy of the Upper Critical Zone in the western Bushveld Complex

The Upper Critical Zone is a *ca*. 500 m thick, distinctly layered interval that can be correlated throughout much of the western and eastern limbs, and part of the northern limb, of the Bushveld Complex. The interval is characterized by the occurrence of so-called cyclic units, consisting of repetitive packages of chromitite-pyroxenite-norite-anorthosite. The cyclic units are characterized by progressively more evolved chemical compositions with height and are thought to have formed in response to magma replenishments to the Bushveld chamber (*e.g.* Eales *et al.*, 1986). PGE mineralised cyclic units include the UG1, the UG2, the Pseudoreefs, as well as the Merensky and Bastard units (Figure 2). The latter is considered, by most workers, to

doi:10.2113/gssajg.111.2-3.159

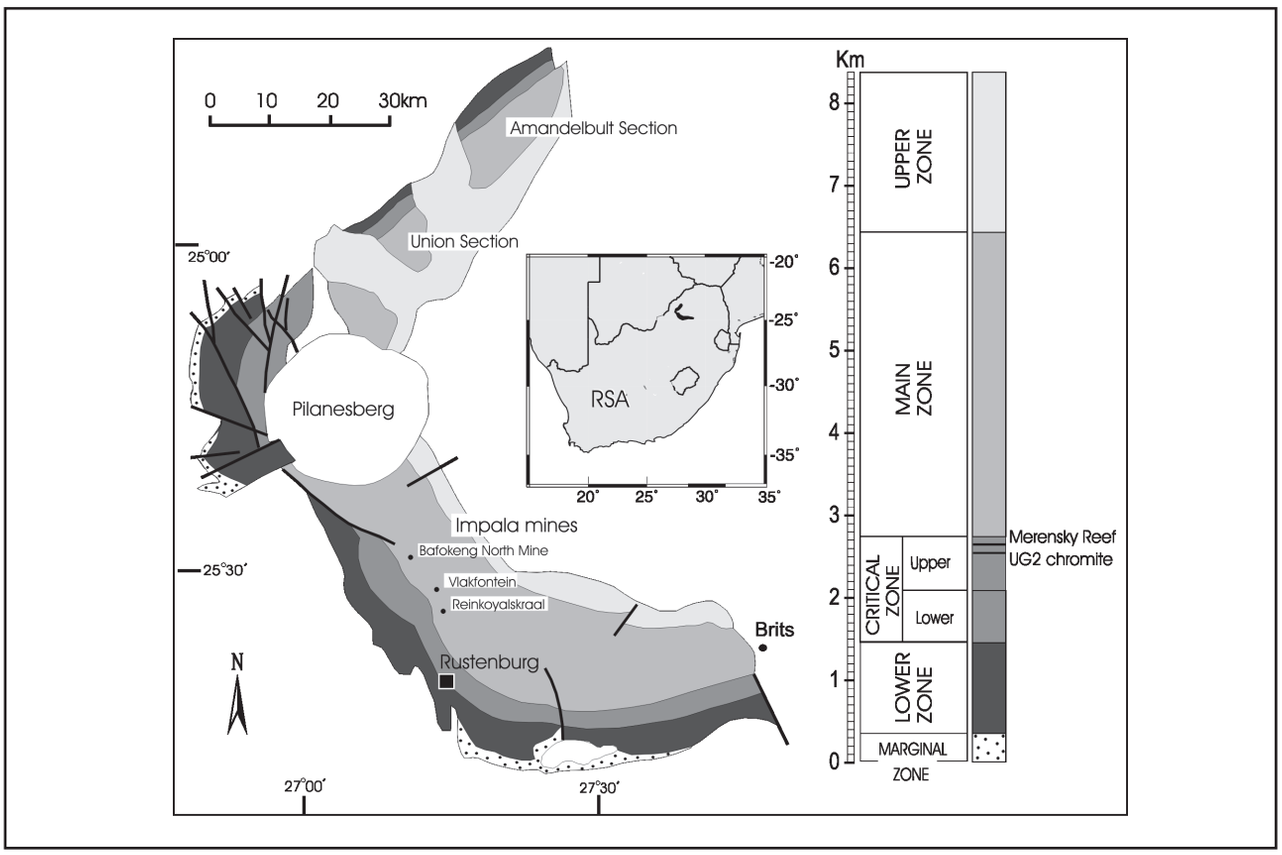

Figure 1. Locality map of the western Bushveld Complex (modified from Godel *et al.*, 2006).

represent the uppermost unit of the Critical Zone, whereas Kruger (2005) suggested that the base of the Main Zone should be placed at the level of the Merensky Reef.

While the cyclic units show remarkable lateral continuity in the western Bushveld, some variation in thickness, lithology and composition is apparently controlled by proximity to the main feeder zone, believed to be located at Union Section (Figure 1, Eales *et al.* 1988, Maier and Eales 1997). In the vicinity of the feeder zone the rocks are relatively magnesian and olivine-rich, and the units may be "beheaded", *i.e.* they lack norites and/or anorthosites. More distal to the feeder the rocks tend to be less magnesian, olivine is rare or absent, and cyclic units tend to be more complete, but the most primitive units, *i.e.* the Pseudoreefs, are poorly developed or absent. Impala mine is located in a transitional position between the proximal and distal facies, and there occur several decimeter-meter thick pyroxenites, harzburgites and troctolites, some of which contain disseminated sulfides, that have been correlated with the Pseudoreefs by Maier and Eales (1997). The present study demonstrates that these layers also occur on the farm Vlafkfontein.

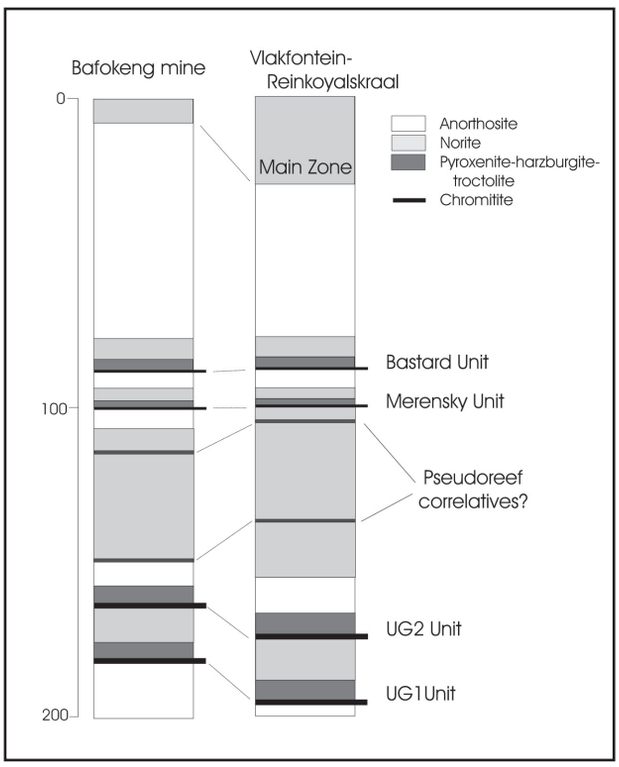

Figure 2. Schematic stratigraphic profiles through the uppermost portion of the Upper Critical Zone at Impala platinum mines. Left profile=northwestern portion of lease area (including Bafokeng mine); Right profile=southeastern portion of lease area (including Vlakfontein and Reinkoyalskraal).

Setting of the Bushveld chromitites

The Bushveld Complex contains up to 14 major chromitite seams and numerous subsidiary layers and

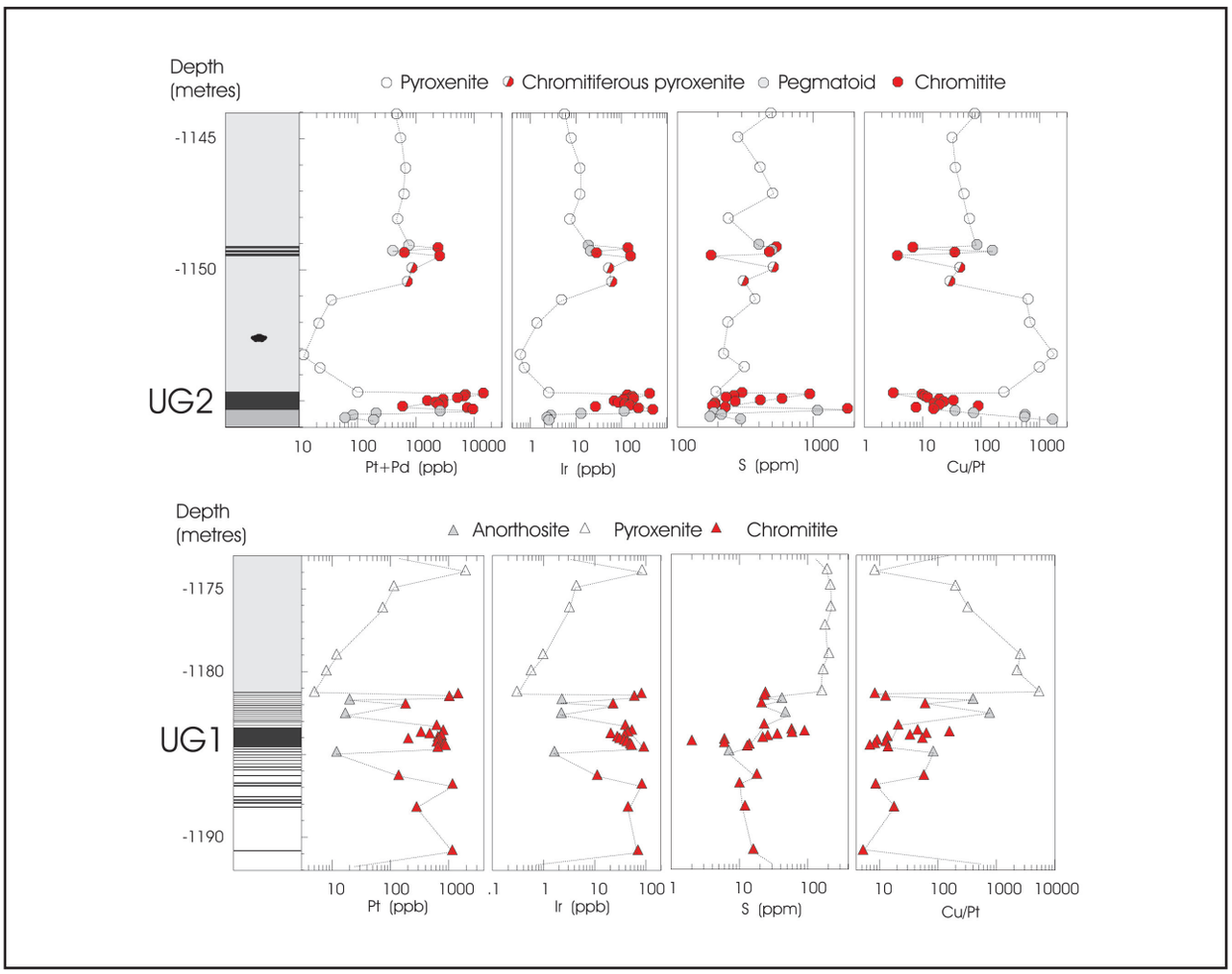

Figure 3. Selected elements and element ratios plotted vs height in the UG1 and UG2 chromitites, Reinkoyalskraal.

stringers. All seams are located in the ca 1 km thick Critical Zone (Figure 1). The chromitites are mainly hosted by orthopyroxenites and, to a lesser extent, by harzburgites, olivine orthopyroxenites, norites and anorthosites. According to standard nomenclature the seams are labeled, from the bottom to the top, as lower group (LG) seams 1 to 7, middle group (MG) seams 1 to 4, and upper group (UG) seams 1 to 3 (Fourie, 1959; Coertze and Schumann, 1962). Regional studies indicate continuity of many of the layers along several tens of km of strike (*e.g.* Cousins and Feringa, 1964; Hatton and von Gruenewaldt, 1987; Scoon and Teigler 1994).

Many of the major seams, *e.g.* the LG6, UG1 and UG2 chromitites, are composite layers consisting of one or two main seams and several subsidiary seams. The subsidiary seams may occur in the hanging wall of the main seam (*e.g.* UG2, Figure 3), in which case they may be called "leader seams" in the mines, and/or its foot wall (*e.g.* UG1, Figure 3). They show varying lateral continuity (meters to kilometers), and may bifurcate and merge with the main seams (*e.g.* Davey, 1992). In the case of both the UG1 and UG2 chromitites the combined thickness of the main and subsidiary seams has been shown to be broadly constant along considerable strike lengths (Davey, 1992; Nex, 2004).

Previously proposed models for the formation of the chromitite layers

The formation of the massive chromitite layers in the Bushveld remains controversial. Several models have been proposed, but none explains all geological and compositional features observed. Perhaps the Bushveld. Perhaps the most widely accepted model involves mixing of relatively differentiated residual magma with relatively magnesian replenishing magma (Irvine, 1975; 1977). This model is consistent with the development of many of the chromitites at the base of cyclic units. Furthermore, in experiments the mixed magma has been shown to have chromite as its first liquidus phase (Sharpe and Irvine, 1983). However, the model predicts a reversal in mineral and whole rock differentiation indexes such as Mg# above the chromitites which is not observed in most cases (Teigler and Eales, 1993).

Gravitational sinking of dense chromite through relatively lighter silicate magma was one of the first models proposed (Wager and Brown, 1968), but other authors have argued that gravitational fractionation of small chromite crystals may be impeded by the yield strength of the magma (Jackson, 1961).

An increase in oxygen fugacity (Ulmer, 1969; Cameron and Desborough, 1969; Snethlage and von

Gruenewaldt, 1977) may reduce the solubility of chromite in the magma, but it is difficult to understand how the oxygen fugacity could have fluctuated at equivalent stratigraphic levels throughout the entire 400 km wide magma chamber. The same constraint applies to models of chromitite formation in response to contamination of the magma with the host rocks, and indeed to the magma mixing and gravitational settling models mentioned above. Moreover, MELTS simulations of contamination of Bushveld magnesian basalt with SiO_2 do not produce liquids that are saturated initially in chromite alone (Mondal and Mathez, 2007).

Mass balance calculations indicate that the Bushveld layered sequence is characterized by an excess of Cr (Maier and Teigler, 1995; Eales, 2000). This has led to the proposal that some of the intruding magmas contained significant amounts of chromite phenocrysts (Eales, 2000; Mondal and Mathez, 2007). De Bremond d'Ars *et al.* (2001) have experimentally simulated entrainment of dense sulfide droplets by ascending, light, silicate magma and thus entrainment of chromite crystals should be realistic too. However, upon emplacement of the magma chromite phenocrysts would have to settle to the floor of the magma chamber to form the chromitite layers and thus the same problem applies as in the original gravity settling model mentioned above.

An increase in pressure (Cameron, 1980; Lipin, 1993; Cawthorn, 2005) represents an elegant model as pressure changes would affect the entire chamber simultaneously. It is possible that the frequent replenishment of the Bushveld chamber with new magma pulses was responsible for multiple earthquakes and venting of the chamber resulting in pressure changes. However, Mondal and Mathez (2007) argue that phase boundaries in systems involving spinel do not appear to be particularly sensitive to pressure.

Nicholson and Mathez (1992) showed that addition of water to a basaltic magma suppresses the crystallization temperatures of silicates relative to that of chromite and suggested that volatile fluxing of semi-consolidated norite and pyroxenite cumulates may have led to the formation of the Merensky chromitite stringers and their anorthositic footwall. Maier and Barnes (2003) applied the model to the chromitites of the Boulder Bed, but the relevance of the mechanism in forming nearly 10 m of combined massive chromitite in the Critical Zone remains uncertain.

PGE contents of the Bushveld chromitites

The most comprehensive work on the PGE distribution in the Bushveld chromitites remains that of Teigler (1990a,b) and Scoon and Teigler (1994) who studied PGE contents in the LGs, MGs and the UG1 at Union Section and in the Brits area, western Bushveld Complex. They built on earlier studies by von Gruenewaldt *et al.* (1986), Naldrett and von Gruenewaldt (1989), and Lee and Parry (1988) that had shown a progressive increase in PGE contents and PPGE/IPGE ratios with height in the Complex. They also showed that PGE contents and PGE ratios in individual seams show considerable lateral continuity (see also von Gruenewaldt and Merkle, 1995, Cawthorn *et al.*, 2002) suggesting little vertical mobility of the PGE. Detailed studies on PGE distribution patterns in the UG2 chromitite have been conducted by McLaren and de Villiers (1982, several localities in the western and eastern lobe), Gain (1985, Maandagshoek), Hiemstra (1986, Western Platinum Mine), and von Gruenewaldt *et al.* (1990). The only detailed studies of the UG1 chromitite remain those of Scoon and Teigler (1994) in the Brits area and von Gruenewaldt *et al.* (1990) in the northeastern Bushveld. Most of these studies identified a distinct distribution pattern of the PGE with peak values at the bottom and the top of the seams (Figure 4). A summary of the published PGE data on Bushveld chromitites (and silicate reefs) can be found in Barnes and Maier (2002b).

Stratigraphy of the examined sequence

The UG1 and UG2 chromitites on the farm Reinkoyalskraal

The farm Reinkoyalskraal 278JQ is situated in the southeastern portion of the Impala Platinum Mines lease area (Figure 1). At this locality, the UG1 is located at a depth of 1183 m. It consists of a 1.1 m thick main chromitite and *ca.* 50 subsidiary chromitite stringers (combined thickness: 91 cm) emplaced within an 8 m anorthosite (Figure 3). The stringers have mostly sharp, but irregular contacts to the anorthosite, in places showing evidence for ductile deformation. The interlayering of anorthosite and chromitite in the footwall of the UG1 is characteristic of both the eastern and western Bushveld (Lee, 1981), *i.e.* along a combined strike length of more than 250 km. The development of anorthosite in the hanging wall of the UG1 chromitite is rather common at Impala mine, but elsewhere in the Bushveld Complex it has previously only been described from Maandagshoek (Gain, 1985). The anorthosite is overlain by *ca.* 8 m of medium grained feldspathic orthopyroxenite that contains several thin chromitite stringers at the top. Next are *ca.* 12 m of leuconorite, 2 m of norite, 40 cm of melanorite, 80 cm of orthopyroxenite with a 1cm chromitite stringer at the top, and 2.2 m of norite. The overlying UG2 unit is of a broadly similar appearance as elsewhere in the western Bushveld Complex. It begins with a 40 cm pegmatoidal pyroxenite overlain by the 66 cm thick UG2 chromitite. The basal contact of the chromitite is undulating and diffuse with dense disseminations of chromite impregnating the uppermost 10 cm of the pegmatoid. In contrast, the top contact of the UG2 chromitite is knife sharp, which is more typical of other localities in the western Bushveld. The UG2 is overlain by 11 m of medium grained feldspathic orthopyroxenite, containing occasional chromitite blebs (Figure 3). Some 5.3 m below the top contact occurs a *ca.* 1.7 m interval of four "leader" chromitite seams (1-14 cm thick) with sharp

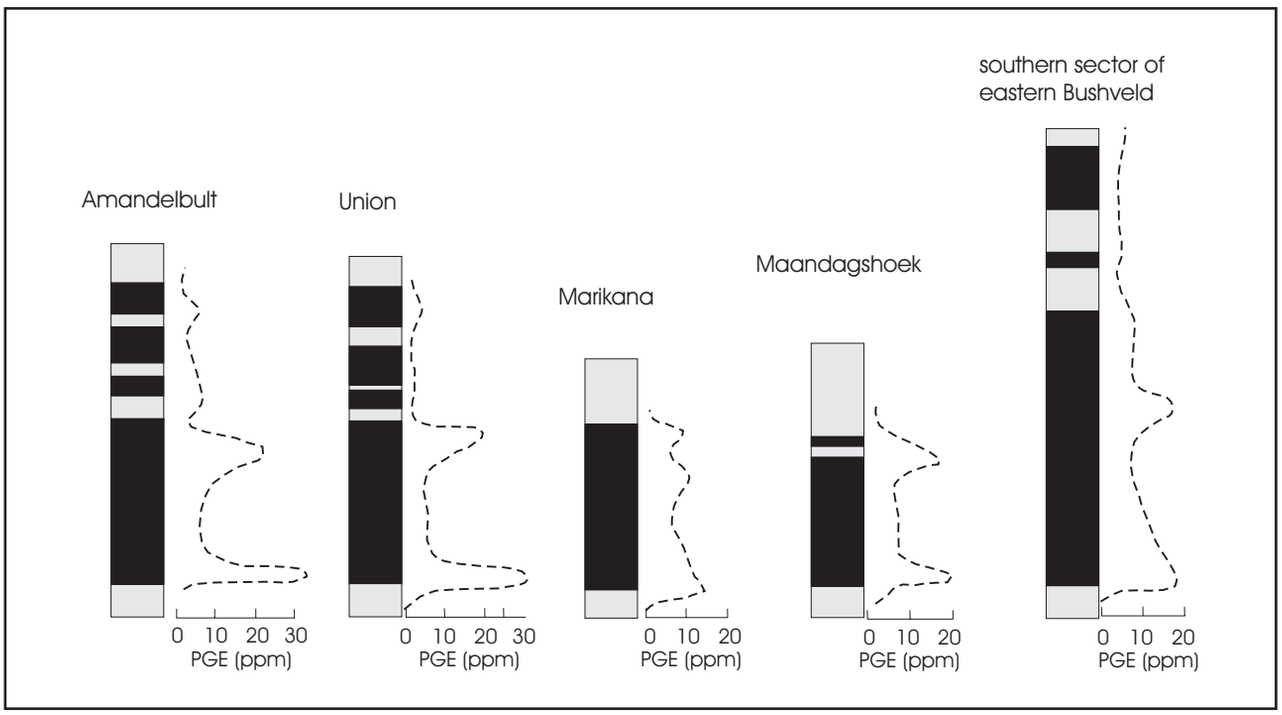

Figure 4. PGE distribution in the UG2 chromitite throughout the Bushveld. Modified after von Gruenewaldt and Hatton (1986).

bottom and top contacts and numerous fine chromitite stringers (Figure 3). A *ca.* 8 cm thick pegmatoidal pyroxenite overlies the uppermost "leader". The UG2 pyroxenite is overlain by 115 m of mostly norite and mottled anorthosite forming the footwall to the Merensky Reef.

The Pseudoreefs

In borehole 3455 at Vlakfontein 276JQ, some 3 km to the northwest of Reinkoyalskraal (Figure 1), a 9 cm thick sulfide-bearing troctolite occurs some 20 m above the top contact of the UG2 pyroxenite, at the base of a mottled anorthosite termed FW 9 in the mine (Leeb-du Toit, 1986). Maier and Eales (1997) described a composite 0.5 m interval of pyroxenite-harzburgite-troctolite at the same position at Bafokeng North mine, a further 5 km to the northwest, and interpreted this to be the correlative of the upper Pseudoreef in the southern limb of the western Bushveld Complex (see their Figure 1.3). The Vlakfontein intersection also contains several harzburgite and pyroxenite layers developed in the immediate footwall of the Boulder Bed (FW6). Harzburgitic and troctolitic layers in broadly equivalent stratgraphic positions are also found at Wildebeestfontein and Bafokeng North mine (Maier and Eales, 1997).

The Bastard reef

As the Bastard reef was severely disturbed by a shearzone in the drillcore on Reinkoyalskraal, it has been sampled on Vlakfontein where it occurs at a depth of 1660m. At this locality, the Merensky hanging wall anorthosite is overlain by a 1 mm chromitite stringer, 2 m of orthopyroxenite, 9 m of norite and 30 m of anorthosite before one passes into a thick sequence of Main Zone norite, gabbronorite and anorthosite that contain thin pyroxenite layers at 1609, 1474, and 1355 m. Visible sulfides occur mainly in a ca 1-5 cm interval at the base of the Bastard Unit.

Methods

All whole rock analyses were conducted at Université du Québec à Chicoutimi (UQAC). The whole rock S contents were determined using a HORIBA EMIA-220V analyser, which uses combustion and infrared analysis. For details of the method and results for reference materials, see Bédard *et al.* (2008).

In the silicate rocks the PGE and Au were collected from 20 g of sample by Ni-sulphide fire assay followed by instrumental neutron activation analysis (INAA), using a slightly modified version of the formula of Steele *et al.* (1975) (Gingras, 2002). Because of the difficulty of dissolving chromites in the standard fire assay flux

Table 1. Comparison of recommended PGE and Au values in chromite and those obtained at University of Quebec, Chicoutimi

	CHR-Bkg			
	UQAC	**1 sigma**	**RV**	**1 sigma**
Au (ppb)	5.54	0.72	4.3	0.731
Ir	7.29	0.58	6.2	0.806
Os	2.11	0.17	1.9	1.292
Pd	99.5	8.0	80.8	12.9
Pt	70	5.6	58	7.0
Rh	4.47	0.18	4.7	0.71
Ru	9.13	0.82	9.2	2.02

RV= Recommended Value (Potts P.J., Gowing C.J.B. and Govindaraju K., 1992)

Table 2. Precision and accuracy of INAA analyses of lithophile elements at UQAC (using in-house standard KPT-1)

	KPT-1 UQAC	1 sigma	AV*	1 sigma
As (ppm)	*2.24*	*0.36*	*2.20*	
Ba	469	23	465	25
Ce	63.8	1.3	55.7	4.7
Co	*74.9*	*1.4*	*77.8*	
Cr	147.1	2.9	152.2	13.7
Cs	4.18	0.19	4.42	0.45
Cu	*1231*	*73*	*1106*	
Eu	1.32	0.04	1.24	0.09
Fe_2O_3 (wt %)	12.49	0.36	12.24	0.19
Hf	4.34	0.19	4.41	0.34
La	26.29	0.55	26.91	1.95
Lu	0.41	0.01	0.42	0.02
Na_2O (wt %)	2.52	0.05	2.61	0.10
Nd	24.97	1.79	24.64	1.35
Ni	*1141*	*103*	*1079*	
Rb	60.5	4.7	61.5	4.4
S (%)	*1.13*	*0.03*	*1.01*	
Sb	11.07	0.42	10.01	0.99
Sc	24.31	0.44	24.84	2.08
Se	2.68	0.24	2.93	0.53
Sm	4.94	0.13	4.90	0.28
Ta	0.54	0.11	0.60	0.059
Tb	0.73	0.08	0.74	0.06
Th	7.65	0.23	7.27	0.68
U	1.74	0.11	1.79	0.18
Yb	2.71	0.07	2.69	0.13
Zn	111	15	120	12

Assigned values: normal type, informational values: italics (Webb *et al.*, 2006)

mixtures, the flux mixture for the chromitites was modified using the formula of Bédard and Barnes (2004). Copper was determined by atomic absorption spectrophotometry. All other elements were determined by INAA using the method of Bédard and Barnes (2002). As an independent check on the quality of the whole rock analyses the UQAC laboratories take part in the International Association of Geoanalysts ongoing proficiency tests. Furthermore, the PGE were determined in the international reference materials CHR-bg (a massive chromitite), and the major and trace elements were determined in KPT-1 (a diorite from Sudbury containing disseminated base metal sulphides) in the same runs as our samples. The reference materials agree with recommended or assigned values within analytical error (Tables 1 and 2).

We analysed 63 half core samples from a drillcore through the UG2 and UG1 chromitites and their foot- and hanging walls, seven samples from the Bastard Reef, and seven samples from the Pseudoreefs. The chromitites were sampled continuously at 5 to 10 cm intervals, but sample spacing was wider in their footwall and hanging wall, with sample sizes usually being 10 to 15 cm. The combined data are presented in Tables 3-4.

Results and Discussion

Distribution of lithophile elements and sulfur

The studied rocks comprise chromitites, ortho-pyroxenites and anorthosites. The relative proportions of chromite and orthopyroxene in our samples can be estimated using a plot of Fe_2O_3 vs Cr_2O_3 (Figure 5a). Note that the pegmatoidal rocks plot along the same chromite-orthopyroxene control line as the medium grained pyroxenites indicating that all rocks formed by predominantly magmatic processes. The anorthosites plot below the opx-chromite tieline, reflecting plagioclase control.

In the plot of Na_2O vs Cr_2O_3 (Figure 5b) one can evaluate the effects of chromite, plagioclase and possibly the trapped liquid fraction (TLF). The anorthosites show enrichment in Na_2O, most of the melanorites and pyroxenites contain between 0.3 and 0.8 weight % Na_2O, and most chromitites have 0.1 to 0.3 weight % Na_2O. Because Upper Critical Zone orthopyroxenes contain <0.1 weight % Na_2O (*e.g.* Maier and Eales, 1997) the measured whole rock Na_2O must be present in another phase, *e.g.* cumulate plagioclase or trapped liquid. In order to decide which, one needs to consider an element that is incompatible with all of the possible cumulate phases, *e.g.* Th or Hf. At the stratigraphic level of the intrusion considered here, the cumulates are thought to have crystallized from the B1 and B2 magma types (Sharpe, 1981). The concentrations of Hf are similar in the B1 and B2 magmas (1.9 vs 1.4 ppm, Curl, 2001). The levels of Th are very different, (3.3 vs 0.6, Curl, 2001). Thus, Hf is better suited to estimate the trapped liquid component. Assuming a Hf value for the mixed magma of 1.7 ppm, the measured Hf concentrations suggest that most of the pyroxenites contain 10-50% trapped liquid fraction (the pegmatoids contain higher trapped liquid fractions). These results suggest that the Na_2O in the pyroxenites represents the TLF. Modeling of the chromitites is not possible because the trace element contents are mostly below the detection limit. Comparison of Th and Hf concentrations also provides some insight into the relative importance of different parental magmas involved in the crystallization of the rocks (Figure 5c). Most of the data plot between the B1 and B2 compositions suggesting a hybrid magma, but with a larger component of B1.

A plot of S versus Cr_2O_3 shows that the UG2, the Pseudoreefs and the UG1 contain less than 0.1 wt % S and many samples contain less S than the B1 or B2 magmas (Figure 5d). The UG1 is particularly poor in S with most samples containing <100 ppm S, whereas the samples from the Bastard unit contain the highest S levels. In order to decide whether there are any cumulate sulphides present in the samples with relatively low S content, one can plot S/La vs Cr_2O_3 (Figure 5e). If the S found in the samples is controlled by the trapped liquid component the S/La ratio of the rocks should be similar to the parent magmas (60 to 20 in the B1 and B2 magmas, respectively). Many UG-1

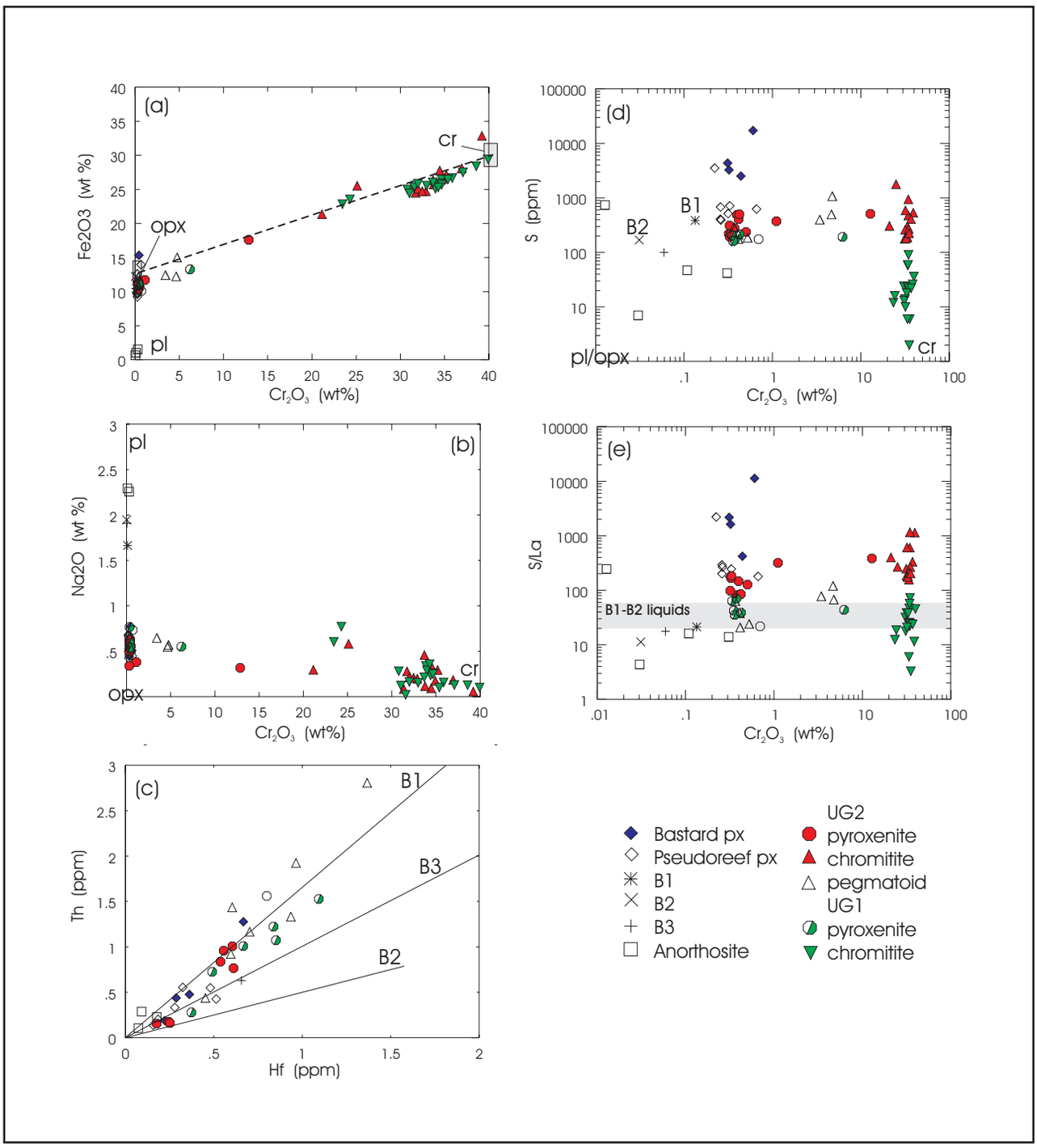

Figure 5. Binary variation diagrams of (**a**) Fe_2O_3 vs Cr_2O_3, (**b**) Na_2O vs Cr_2O_3, (**c**) Th vs Hf, (**d**) S vs Cr_2O_3, and (**e**) S/La vs Cr_2O_3. Compositions of orthopyroxene and chromite in (**a**) are from Maier and Eales (1997) and Teigler and Eales (1996). Compositions of B1-B3 liquids are from Curl (2001).

samples have low S/La and hence would not appear to contain cumulate S, but most other samples have S/La considerably greater than the magma indicating that cumulate sulphides are present.

In summary, the components of the chromitites are cumulus chromite, cumulus orthopyroxene, <*ca*. 10% TLF and, in the UG-2 chromitite, a small fraction of cumulus sulphides. The components of the pyroxenites are cumulus orthopyroxene and minor chromite and sulphides, with a large range in trapped liquid fraction (10 to 50%). The components of the anorthosites are largely cumulus plagioclase with <10% trapped liquid fraction.

Distribution of platinum-group elements

In the analysed section, the UG1 chromitite contains 628 ppb Pt, 13 ppb Pd, 265 ppb Ru, and 45 ppb Ir over 112 cm. Most of these values are similar to those reported for the UG1 by von Gruenewaldt *et al.* (1986) and Scoon and Teigler (1994), except for Pd which is

Table 3. Whole-rock compositional data for UG1 and UG2 units.

Sample	Rock type	Location	Height	Fe_2O_3 wt%	Na_2O wt%	Cr_2O_3 wt%	Co ppm	Sc ppm	Zn ppm	Cu ppm	Ni ppm	S ppm	Os ppb	Ir ppb	Ru ppb	Rh ppb	Pt ppb
G2-01	Px	ug-2	1144.04	11.55	0.576	0.40	84	29	119	27	592	488	3.5	5.62	12	8.4	348
G2-02	Px	ug-2	1144.95	10.92	0.587	0.37	80	28	111	14	572	280	5.7	7.85	22	13	439
G2-03	Px	ug-2	1146.10	11.30	0.633	0.41	83	28	160	19	577	408	4.4	12.2	40	20	522
G2-04	Px	ug-2	1147.09	11.29	0.607	0.42	82	29	121	22	569	503	5.2	12.2	41	20	432
G2-05	Px	ug-2	1148.04	na	na	na	na	na	na	24	618	238	2.3	7.37	21	20	378
G2-06	Peg-Px	ug-2	1149.04	12.41	0.647	3.44	101	28	154	40	856	399	9.5	18.7	50	49	472
G2-07	Cr	ug-2	1149.14	32.86	0.056	39.22	318	12	798	12	1522	535	71	139	545	na	1771
G2-08	Peg-Px	ug-2	1149.25	12.23	0.548	4.66	101	25	147	45	915	499	14.1	20.9	82	28	288
G2-09	Cr	ug-2	1149.32	27.78	0.093	34.47	273	10	710	15	1480	477	13	28.3	145	na	423
G2-10	Cr	ug-2	1149.45	25.40	0.084	31.36	245	11	752	8	1490	178	81	160	583	na	2181
G2-11	Px+Cr	ug-2	1149.91	17.61	0.318	12.86	156	23	328	33	946	511	22	52.9	176	240	763
G2-12	Px+Cr	ug-2	1150.43	21.37	0.296	21.13	199	17	509	19	936	307	31	61.9	275	112	649
G2-13	Px	ug-2	1151.11	11.71	0.380	1.11	90	27	113	23	633	374	2.6	4.81	<9	9.0	36
G2-14	Px	ug-2	1152.00	10.60	0.557	0.50	80	26	102	15	552	237	<.62	1.39	<8	<1.8	22
G2-15	Px	ug-2	1153.20	10.36	0.625	0.32	79	26	89	20	544	220	<.67	0.6	5	<2.2	12
G2-16	Px	ug-2	1153.70	11.18	0.501	0.33	86	27	110	23	595	312	<1.3	0.73	<6	2.0	23
G2-17	Px	ug-2	1154.65	11.14	0.340	0.33	88	28	121	22	606	193	1.1	2.52	8	16	89
G2-18	Cr	ug-2	1154.69	26.34	0.458	33.70	260	11	676	36	906	300	321	422	1319	na	11457
G2-19	Cr	ug-2	1154.74	26.40	0.318	34.59	259	11	650	40	959	941	111	137	743	na	4134
G2-20	Cr	ug-2	1154.80	24.50	0.279	31.73	245	10	677	33	974	261	104	176	689	na	3062
G2-21	Cr	ug-2	1154.86	na	na	na	na	na	na	36	1009	229	112	186	712	na	2967
G2-22	Cr	ug-2	1154.91	25.09	0.212	32.01	246	11	622	35	1000	590	57	112	407	na	1807
G2-23	Cr	ug-2	1154.97	28.09	0.183	36.94	280	11	722	36	1059	409	34	69.9	229	na	1077
G2-24	Cr	ug-2	1155.02	26.56	0.173	34.93	266	10	683	34	1038	268	48	86.1	266	na	1483
G2-25	Cr	ug-2	1155.08	24.73	0.197	32.89	248	9	639	31	1064	190	63	119	391	na	1980
G2-26	Cr	ug-2	1155.13	25.71	0.116	33.76	255	10	644	31	1130	190	97	153	618	na	1600
G2-27	Cr	ug-2	1155.19	24.71	0.208	32.48	247	9	644	35	1048	182	23	27	164	na	393
G2-28	Cr	ug-2	1155.24	27.15	0.294	35.20	268	10	700	38	1101	226	147	239	1002	na	4941
G2-29	Cr	ug-2	1155.29	25.53	0.580	25.12	221	11	563	90	1227	1785	252	494	1543	na	5863
G2-30	Peg-Px	ug-2	1155.36	15.00	0.568	4.76	115	27	214	64	881	1076	67	116	327	na	1780
G2-31	Peg-Px	ug-2	1155.44	11.43	0.527	0.53	89	28	104	9	734	186	7.6	13.0	38	26	121
G2-32	Peg-Px	ug-2	1155.52	12.14	0.554	0.41	89	29	102	17	654	212	1.9	2.78	7	6.0	30
G2-33	Peg-Px	ug-2	1155.60	10.88	0.676	0.41	80	30	128	14	598	175	1.5	2.33	<8	3.7	25
G2-34	Peg-Px	ug-2	1155.70	10.97	0.652	0.37	82	28	109	27	631	293	1.7	2.53	<7	5.6	16
G1-29	Px	ug-1	1173.85	13.27	0.551	6.23	112	24	211	16	628	193	44.9	84.5	173	204	1937
G1-28	Px	ug-1	1174.80	11.22	0.542	0.43	84	29	144	23	581	215	2.3	4.34	21	8.2	115
G1-27	Px	ug-1	1176.10	10.94	0.573	0.34	82	26	111	24	568	219	1.5	3.17	20	5.0	74
G1-26	Px	ug-1	1177.22	na	na	na	na	na	na	27	585	180	<7.9	4.92	<18	13	133
G1-25	Px	ug-1	1178.93	10.93	0.547	0.35	81	28	107	31	572	205	<.68	0.97	4	3.8	12
G1-01	px	ug-1	1179.90	10.89	0.598	0.38	82	27	90	18	569	169	<1.4	0.57	<6	2.1	8
G1-02	Px	ug-1	1181.18	11.02	0.767	0.36	76	28	74	27	507	161	<1.3	0.3	<7	0.6	5
G1-03	Cr	ug-1	1181.29	24.99	0.281	30.79	242	11	689	12	811	24	56	81.9	299	na	1449
G1-04	Cr	ug-1	1181.45	25.76	0.340	33.88	261	11	802	13	839	23	44	59.5	292	na	1025
G1-05	An	ug-1	1181.64	1.55	2.258	0.31	10	3	29	8	41	42	<1.2	2.28	<15	1.1	20
G1-06	Cr	ug-1	1181.91	26.47	0.258	34.67	271	10	744	11	868	21	19	22.8	143	na	183
G1-07	An	ug-1	1182.48	1.04	2.292	0.11	6	2	17	13	18	47	1.2	2.22	8	1.7	17
G1-08	Cr	ug-1	1183.20	25.89	0.236	34.39	268	10	730	13	902	23	40	39.5	277	na	621
G1-09	Cr	ug-1	1183.50	25.10	0.288	33.98	266	10	710	36	905	58	53	53.5	344	na	804
G1-10	Cr	ug-1	1183.60	25.70	0.249	34.68	270	11	785	53	949	90	39	44.5	325	na	336
G1-11	Cr	ug-1	1183.70	25.28	0.358	34.29	264	10	810	30	926	59	19	20.6	144	na	474
G1-12	Cr	ug-1	1183.80	29.42	0.100	39.94	312	12	896	25	929	36	41	38.4	261	na	753
G1-13	Cr	ug-1	1183.90	28.41	0.128	38.59	298	11	837	9	993	26	25	27.7	171	na	658
G1-14	Cr	ug-1	1184.00	27.50	0.130	37.09	281	12	777	11	961	22	29	30.8	209	na	203
G1-15	Cr	ug-1	1184.10	26.67	0.157	35.87	274	11	808	6	898	6	36	37.4	182	na	662
G1-16	Cr	ug-1	1184.20	26.46	0.100	35.38	264	11	717	8	934	2	43	42.4	218	na	626
G1-17	Cr	ug-1	1184.31	26.03	0.215	33.68	254	10	966	7	870	6	52	49.6	275	na	844
G1-18	Cr	ug-1	1184.41	25.32	0.022	31.57	249	10	1012	6	862	14	43	52.5	309	na	880
G1-19	Cr	ug-1	1184.52	24.43	0.123	31.04	239	9	871	9	789	13	65	91.5	444	na	647
G1-20	An	ug-1	1184.81	0.67	3.193	0.030	3	1	146	1	22	7	0.7	1.62	6	1.0	12
G1-21	Cr	ug-1	1186.22	25.57	0.154	32.99	261	10	780	8	891	18	9	11.2	82	64	139
G1-22	Cr	ug-1	1186.75	25.82	0.162	31.99	257	10	931	10	887	10	71	83.6	381	505	1164
G1-23	Cr	ug-1	1188.13	22.84	0.604	23.45	212	7	1029	5	606	12	40	44.6	254	66	282
G1-24	Cr	ug-1	1190.75	23.54	0.771	24.31	218	7	1171	6	499	16	61	70.1	270	466	1151

Px = pyroxenite; An = anorthosite; Hz = harzburgite; Peg = pegmatoid; Cr = chromitite; Troct=troctolite

Pd	Au	As	Sb	La	Ce	Nd	Sm	Eu	Tb	Yb	Lu	Ba	Cs	Hf	Rb	Ta	Th	U
ppb	ppb	ppm	ppm	ppm	ppm	ppm	ppm	ppm	ppm	ppm	ppm	ppm	ppm	ppm	ppm	ppm	ppm	ppm
121	6.2	<0.5	0.13	3.31	7.79	4.7	0.76	0.21	0.12	0.73	0.12	86	<0.2	0.61	3.90	0.04	0.77	<0.06
108	2.6	<0.5	0.08	3.43	6.85	3.0	0.68	0.22	0.11	0.65	0.11	64	0.12	0.54	3.05	0.06	0.84	0.08
153	4.3	<0.5	0.18	4.85	8.64	3.9	0.77	0.22	0.10	0.62	0.12	72	<0.2	0.56	3.12	0.09	0.96	0.36
203	2.8	<0.5	<0.05	5.92	12.88	5.9	1.12	0.30	0.15	0.72	0.12	76	0.16	0.60	3.62	0.08	1.01	0.35
112	0.9	na	na	na	na	na	na	na	na	na	na	na	na	na	na	na	na	na
291	10.9	2.6154	0.59	5.15	8.72	5.0	0.88	0.23	0.10	0.64	0.09	82	0.25	0.94	4.11	0.12	1.33	0.28
644	17.6	13.8866	0.93	0.47	<20	<15	0.12	<0.15	<0.5	<0.2	<0.1	<50	<0.2	<0.6	<5	<0.1	<0.3	0.24
115	26.0	1.8773	0.34	4.16	10.38	3.8	0.74	0.20	0.09	0.53	0.07	78	0.70	0.45	5.30	0.09	0.44	<0.2
215	28.1	4.1712	1.79	0.41	<7	<15	0.07	<0.3	<0.5	<0.2	<0.1	<50	<0.2	<0.6	<5	<0.1	<0.3	<0.2
399	63.0	50.2365	1.21	0.72	<6	<15	0.15	<0.3	<0.5	<0.2	<0.1	<50	<0.2	<0.6	<5	<0.1	<0.3	<0.2
97	13.4	<0.5	0.19	1.33	3.39	<15	0.31	<0.3	<0.5	0.30	0.04	26	<0.2	<0.6	<5	<0.1	<0.1	<0.2
70	2.5	<0.5	0.71	0.77	<5	<15	0.17	<0.3	<0.5	0.22	<0.1	<50	<0.2	<0.6	<5	<0.1	<0.1	<0.2
<15	0.6	<0.5	0.08	1.17	2.26	<15	0.36	0.13	0.08	0.52	0.08	39	<0.2	0.15	<5	<0.1	<0.1	<0.06
<9.2	0.9	1.4357	0.52	1.86	4.04	2.3	0.43	0.17	0.06	0.46	0.08	57	0.23	0.24	<5	<0.1	0.18	0.08
<3.3	0.9	<0.5	<0.05	2.24	5.74	1.8	0.40	0.21	<0.5	0.46	0.08	26	<0.2	0.18	<5	<0.1	0.16	<0.1
<3.1	0.5	<0.5	<0.05	1.86	3.99	2.1	0.44	0.17	0.08	0.52	0.09	42	<0.2	0.25	<5	<0.1	0.16	<0.07
12	0.5	<0.5	<0.05	1.05	2.31	<2	0.32	0.11	0.05	0.44	0.08	19	<0.2	0.21	<5	<0.1	<0.1	<0.07
2944	15.7	<0.5	<0.1	1.92	6.02	<15	0.30	<0.3	<0.5	<0.2	<0.1	<50	<0.2	<0.4	<5	<0.1	<0.3	<0.2
2970	28.2	<0.5	<0.1	1.55	5.76	<15	0.26	<0.3	<0.5	<0.2	<0.1	43	<0.2	<0.4	<5	<0.1	<0.3	<0.2
3702	16.2	<0.5	<0.1	1.40	<5	<15	0.22	<0.3	<0.5	0.08	<0.1	<50	<0.2	<0.4	<5	<0.1	<0.3	<0.2
2219	<10	<0.5	<0.1	<0.3	<5	<15	<0.1	<0.3	<0.5	<0.2	<0.1	<50	<0.2	<0.4	<5	<0.1	<0.3	<0.2
1129	<10	<0.5	<0.1	0.97	<5	<15	0.15	<0.3	<0.5	<0.2	<0.1	<50	<0.2	<0.4	<5	<0.1	<0.3	<0.2
513	<10	<0.5	<0.1	1.22	<5	<15	0.20	<0.3	<0.5	<0.2	<0.1	<50	<0.2	<0.4	<5	<0.1	<0.3	<0.2
701	<10	<0.5	<0.1	1.01	<5	<15	0.16	<0.3	<0.5	<0.2	<0.1	<50	<0.2	<0.4	<5	<0.1	<0.3	<0.2
952	<10	<0.5	<0.1	1.06	<5	<15	0.18	<0.3	<0.5	<0.2	<0.1	<50	<0.2	<0.4	<5	<0.1	<0.3	<0.2
863	<10	<0.5	<0.1	0.90	<5	<15	0.16	<0.3	<0.5	<0.2	<0.1	<50	<0.2	<0.4	<5	<0.1	<0.3	<0.2
200	<10	<0.5	<0.1	1.04	<5	<15	0.16	<0.3	<0.5	<0.2	<0.1	<50	<0.2	<0.4	<5	<0.1	<0.3	<0.2
2746	<10	<0.5	<0.1	1.11	<5	<15	0.19	<0.3	<0.5	<0.2	<0.1	<50	<0.2	<0.4	<5	<0.1	<0.3	<0.2
3641	<10	<0.5	<0.1	6.66	<20	<15	0.64	<2	<0.5	<0.2	<0.1	49	<0.2	<0.4	<5	<0.1	<1	<0.2
841	<10	1.0109	0.22	15.99	30.07	6.9	1.32	0.25	<0.5	0.89	0.13	132	0.28	1.37	<5	0.43	2.81	1.47
88	1.8	0.8915	0.13	7.70	23.99	11.9	2.28	0.33	0.17	0.75	0.11	118	0.12	0.60	4.11	0.15	1.43	0.46
54	1.6	0.775	0.11	10.25	18.78	4.0	1.09	0.24	0.15	0.94	0.15	115	0.49	0.96	13.79	0.15	1.92	1.04
37	1.5	0.2881	0.08	4.64	10.45	3.9	0.95	0.28	0.13	0.76	0.12	88	0.26	0.60	8.51	0.08	0.92	0.33
174	3.4	0.4346	0.07	4.62	10.86	4.7	0.99	0.27	0.14	0.73	0.11	72	0.32	0.70	9.51	0.06	1.17	0.30
608	2.3	0.5721	0.11	4.41	8.46	3.7	0.66	<0.3	0.07	0.58	0.07	58	<0.2	0.67	7.68	<0.1	1.01	0.21
26	1.0	0.5933	0.10	5.54	11.75	5.4	1.04	0.25	0.16	0.71	0.12	85	0.46	0.85	12.72	0.07	1.07	0.35
13	0.9	0.3766	0.05	3.43	8.28	2.5	0.65	0.22	0.13	0.56	0.10	66	<0.2	0.49	9.01	0.06	0.73	0.26
23	1.1	na	na	na	na	na	na	na	na	na	na	na	na	na	na	na	na	na
8	1.9	0.6745	0.09	4.84	11.38	5.2	1.00	0.24	0.18	0.72	0.12	80	0.72	1.09	15.46	0.12	1.53	0.38
3	0.9	<0.5	0.08	2.40	5.37	2.2	0.49	0.20	0.09	0.54	0.08	47	<0.2	0.37	<5	0.04	0.28	<0.2
5	4.3	0.819	0.18	4.55	11.42	3.4	0.87	0.29	<0.5	0.65	0.11	61	<0.2	0.84	<5	0.18	1.22	0.22
71	<10	<0.5	0.45	0.76	<10	<15	0.22	<0.6	<0.5	<0.2	<0.1	<50	<0.2	<0.4	<5	<0.4	<1	<1
30	<10	<0.5	0.26	0.90	<10	<15	0.24	<0.6	<0.5	<0.2	<0.1	<50	<0.2	<0.4	<5	<0.4	<1	<1
<7	0.8	<0.5	0.06	3.00	6.81	2.2	0.40	0.47	0.03	0.14	0.02	91	<0.2	0.09	1.20	<0.4	0.29	0.07
<14	<10	<0.5	0.13	0.86	<10	<10	0.19	<0.6	<0.5	<0.2	<0.1	<50	<0.2	<0.4	<5	<0.4	<1	<1
<7.5	0.7	<0.5	0.09	2.92	6.32	2.3	0.40	0.44	0.02	0.15	0.02	70	<0.2	0.18	<5	0.02	0.23	0.08
14	<10	<0.5	0.30	1.05	<10	<20	0.20	<0.6	<0.5	<0.2	<0.1	<50	<0.2	<0.4	<5	<0.4	<1	<1
<14	<10	<0.5	0.37	1.24	<10	<20	0.24	<0.6	<0.5	<0.2	<0.1	<50	<0.2	<0.4	<5	<0.4	<1	<1
7	<10	<0.5	0.31	1.25	<10	<20	0.24	<0.6	<0.5	<0.2	<0.1	<50	<0.2	<0.4	<5	<0.4	<1	<1
6	<10	<0.5	0.35	1.03	<10	<20	0.22	<0.6	<0.5	<0.2	<0.1	<50	<0.2	<0.4	<5	<0.4	<1	<1
16	<10	<0.5	<0.1	0.79	<10	<20	0.15	<0.6	<0.5	<0.2	<0.1	<50	<0.2	<0.4	<5	<0.4	<1	<1
3	<10	<0.5	0.10	2.26	<10	<20	0.55	<0.6	<0.5	0.13	<0.1	<50	<0.2	0.41	<5	<0.4	<1	<1
5	<10	<0.5	0.09	0.93	<10	<20	0.24	<0.6	<0.5	<0.2	<0.1	<50	<0.2	<0.4	<5	<0.4	<1	<1
9	<10	<0.5	<0.1	<0.3	<10	<20	0.12	<0.6	<0.5	<0.2	<0.1	<50	<0.2	<0.4	<5	<0.4	<1	<1
11	<10	<0.5	0.15	0.61	<10	<20	0.14	<0.6	<0.5	<0.2	<0.1	<50	<0.2	<0.4	<30	<0.4	<1	<1
25	<10	0.4018	0.39	1.00	<10	<20	0.10	<0.6	<0.5	<0.2	<0.1	<50	<0.2	<0.4	0.00	<0.4	<1	<1
39	<10	0.4558	0.67	0.36	<10	<20	0.13	<0.6	<0.5	<0.2	<0.1	<50	<0.2	<0.4	<15	<0.4	<1	<1
19	<10	0.6158	0.29	0.73	<10	<20	0.13	<0.6	<0.5	<0.2	<0.1	<50	<0.2	<0.4	<3	<0.4	<1	<0.2
<3.9	0.3	<0.5	0.14	1.60	4.58	<20	0.14	0.35	<0.1	0.04	<0.1	102	0.80	<0.4	28.29	<0.4	0.07	<0.2
<5.4	<10	0.6752	0.38	0.47	<10	<20	0.13	<0.6	<0.1	<0.2	<0.1	<50	<0.2	<0.4	<3	<0.4	<1	<0.2
27	<10	0.6001	0.81	0.48	<10	<20	0.11	<0.6	<0.1	<0.2	<0.1	<50	<0.2	<0.4	<3	<0.4	<1	<0.2
17	<10	0.3688	0.17	0.97	<10	<20	0.15	<0.6	<0.1	<0.2	<0.1	<50	<0.2	<0.4	<3	<0.4	<1	<0.2
109	<10	1.1772	0.14	0.86	<10	<20	0.17	<0.6	<0.1	<0.2	<0.1	<50	<0.2	0.17	<3	<0.4	<1	<0.1

Table 4. Whole-rock compositional the Bastard and Pseudoreef units

Sample	**B-7**	**B-6**	**B-5**	**B-4**	**B-3**	**B-2**	**B-1**	**PR-7**	**PR-6**	**PR-5**	**PR-4**	**PR-3**	**PR-2**	**PR-1**
Rock type	**px**	**px**	**px**	**px**	**px**	**px**	**an**	**Hz-Peg**	**Hz-Peg**	**px**	**px**	**px**	**px**	**Troct**
Location	**bastard**	**bastard**	**bastard**	**bastard**	**bastard**	**bastard**	**bastard**	**pseudo**	**pseudo**	**pseudo**	**pseudo**	**pseudo**	**pseudo**	**pseudo**
Height	**1663.15**	**1664.06**	**1664.95**	**1665.54**	**1665.62**	**1665.64**	**1665.70**	**1691.74**	**1693.06**	**1694.75**	**1698.39**	**1698.60**	**1699.44**	**1747.00**
Fe_2O_3 (wt%)	na	na	15.35	11.40	11.52	11.71	1.52	13.97	12.62	9.60	10.09	9.24	9.81	9.75
Na_2O	na	na	0.771	0.447	0.465	0.509	2.221	0.448	0.499	0.665	0.521	0.425	0.535	0.680
Cr_2O_3	na	na	0.441	0.324	0.312	0.604	0.013	0.663	0.260	0.259	0.317	0.262	0.330	0.223
Co (ppm)	na	na	118	90	94	118	11	144	123	76	81	81	79	107
Sc	na	na	40	30	28	26	3	11	17	24	26	21	27	7
Zn	na	na	119	101	104	103	15	158	117	101	104	107	100	150
Cu	896	154	282	427	603	1774	133	17	19	20	19	12	18	301
Ni	1963	684	812	997	1235	3468	177	1572	1326	600	611	723	566	1587
S	9426	2043	2511	3252	4379	17191	740	626	682	406	514	393	719	3529
Os (ppb)	<5.5	<4.9	1.3	1.8	3.3	26.4	0.5	1.1	0.3	<.74	<.79	<.67	<.77	1.6
Ir	1.85	0.56	0.78	1.82	2.97	20.90	1.35	1.75	0.27	0.39	0.39	0.56	0.49	2.01
Ru	16	<9	9	15	8	155	2	10	2	8	8	<4.9	<4.7	4
Rh	4.20	0.90	0.98	1.47	2.24	32.12	3.72	5.26	2.06	0.72	0.70	3.20	0.46	4.18
Pt	101	<28	16	24	49	403	49	43	15	7	7	13	7	265
Pd	77	20	10	12	17	347	27	11	5	3	6	12	6	254
Au	79.5	10.9	22.8	29.5	50.6	195.5	16.5	2.7	2.8	2.2	3.2	3.2	3.2	105.9
As (ppm)	<0.5	<0.5	<0.5	<0.5	<0.5	<0.5	<0.5	<0.5	<0.5	<0.5	<0.5	<0.5	<0.5	<0.5
Sb	na	na	<0.05	<0.05	0.04	0.04	0.01	0.04	<0.05	0.02	0.03	<0.05	<0.05	<0.05
La	na	na	5.97	2.00	2.01	1.52	3.01	3.47	2.33	2.03	2.92	1.47	2.92	1.59
Ce	na	na	12.19	4.38	3.85	3.52	6.52	6.45	5.20	3.64	6.56	2.91	7.21	3.55
Nd	na	na	5.0	1.4	1.3	2.3	1.6	3.1	3.0	2.5	4.2	1.3	3.6	<2
Sm	na	na	1.10	0.43	0.40	0.36	0.31	0.54	0.52	0.44	0.64	0.28	0.70	0.26
Eu	na	na	0.25	0.16	0.16	<0.6	0.41	0.21	0.20	0.21	0.20	0.15	0.25	0.20
Tb	na	na	0.18	0.09	0.06	<0.1	<0.1	0.07	0.08	0.09	0.11	0.05	0.10	0.03
Yb	na	na	0.84	0.52	0.48	0.45	0.09	0.33	0.38	0.47	0.50	0.33	0.52	0.18
Lu	na	na	0.15	0.09	0.08	0.08	0.01	0.05	0.06	0.08	0.07	0.05	0.08	0.03
Ba	na	na	70	<50	28	22	82	40	39	36	39	17	36	37
Cs	<0.2	<0.2	<0.2	<0.2	<0.2	<0.2	0.14	<0.2	<0.2	<0.2	<0.2	<0.2	<0.2	<0.2
Hf	na	na	0.67	0.36	0.29	0.22	0.07	0.32	0.28	0.18	0.48	0.15	0.51	0.16
Rb	na	na	7.88	<3	<3	2.49	<3	<3	<3	1.40	1.43	<3	2.25	<3
Ta	na	na	0.10	<0.05	0.04	<0.05	<0.4	0.06	0.05	<0.1	0.04	<0.03	0.04	<0.03
Th	na	na	1.28	0.48	0.44	0.19	0.11	0.56	0.33	0.20	0.55	<0.2	0.43	0.14
U	na	na	0.35	0.09	<0.1	<0.1	<0.1	0.09	0.11	0.08	0.13	<0.06	0.08	<0.06

highly depleted in our section. The footwall and hanging wall stringers have broadly similar PGE contents as the main seam.

The UG2 chromitite contains significantly higher PGE contents, *i.e.* 2111 ppb Pt, 1214 ppb Pd, 362 ppb Ru, and 98 ppb Ir over 66 cm, equivalent to other UG2 intervals analysed previously (McLaren and de Villiers 1982, Hiemstra 1986, Gain 1985). PGE are also elevated in the pegmatoid below the UG2, particularly in the uppermost *ca.* 10 cm, below which values drop sharply. The decrease in PGE content with depth is most systematic in the case of the IPGE and Pt, with Pd behaving more irregularly. As a result, Pt/Pd ratios in the UG2 footwall pegmatoid are significantly lower than in the UG2.

The PGE contents of the UG2 pyroxenite are mostly significantly higher than those of the UG1 pyroxenite, broadly mirroring the variation of PGE contents in the chromitite seams.

Amongst the troctolitic and ultramafic rocks in the footwall of the Merensky Reef that may be correlatives of the Pseudoreefs, the lowermost (troctolitic) sample contains ca 700 ppb PGE+Au, whereas the remainder of the samples contains <50 ppb PGE+Au.

The Bastard Reef has *ca.* 1 ppm PGE +Au over 5 cm. Some sulfides have percolated into the immediate anorthositic floor rocks of the Bastard chromitite (Table 4, Figure 6), as has also been observed at Rustenburg platinum mine (Lee, 1983). In the overlying pyroxenites, PGE contents reach a maximum of *ca.* 200 ppb.

Looking at the combined chalcophile element data, it is apparent that Cu and Au are controlled by sulphides, as indicated by well defined positive correlations with S (Figure 7a-b). In samples with >*ca.* 0.2 weight % sulphides (*i.e. ca.* 1000 ppm S) Ni is equally largely controlled by sulfide, but in the remainder of the samples, chromite and orthopyroxene control Ni (Figure 7c). Surprisingly, none of the PGE

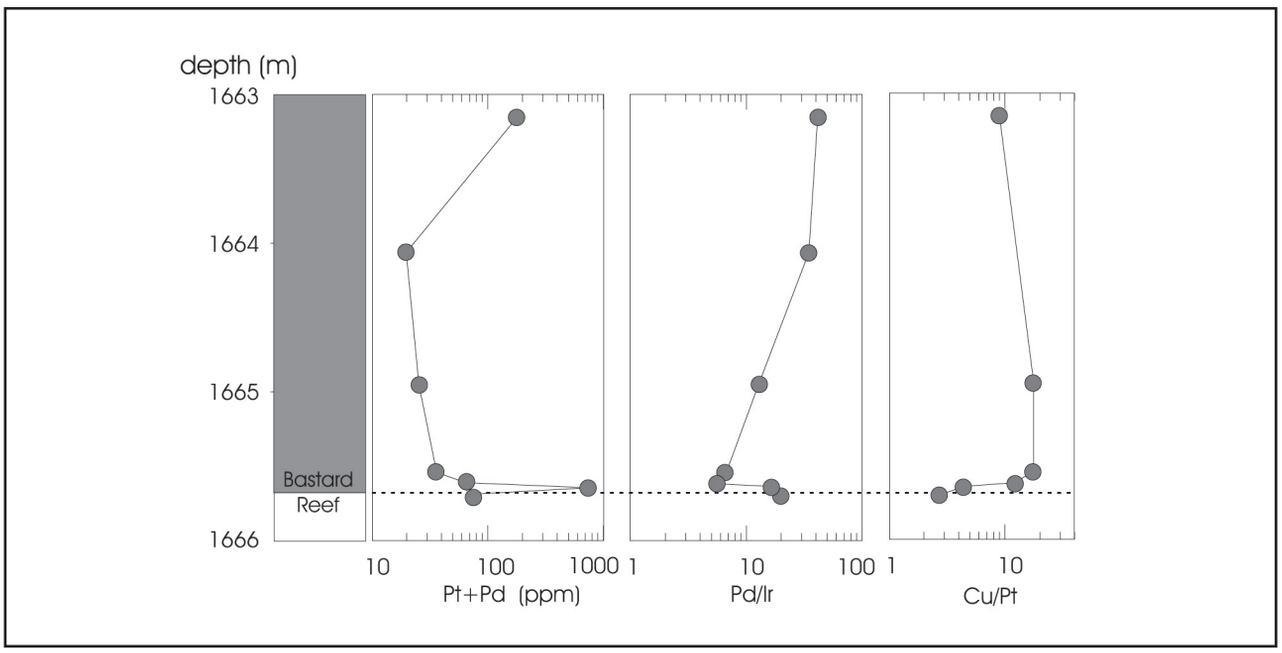

Figure 6. Compositional variation through the base of the Bastard Unit. Note that Pt and Pd have infiltrated into the immediate anorthositic footwall rocks of the reef. See text for further discussion.

show a correlation with S in our rocks, with the exception of the Bastard unit (Figure 7d-f). The question thus arises what other phase(s) could be controlling the PGE. Chromite exerts control on some partially chalcophile elements *e.g.* Co (Figure 8a), and chromite has been suggested to control the IPGE (Righter *et al.* 2004). However, plots of Cr vs Ir or Ru show no significant correlations (Figure 8b-c). Thus chromite does not appear to control the PGE in the present rocks.

The PGE could be largely present in PGM. The PGM mineralogy of the UG-2 chromitite at Impala mine comprises laurite, cooperite, braggite, vysotskite and isoferroplatinum (McLaren and de Villiers, 1982). In the UG1 the dominant phase is laurite, with additional irarsite, Pt-S, Pt, and Pt-Rh-S associated with interstitial chalcopyrite and pentlandite (Merkle, 1992; Maier *et al.*, 2000). The importance of laurite in controlling the bulk of the IPGE is consistent with the good correlation between Ru and Os and Ir (Figure 9a-b). There is no correlation between Sb or As with Pd and Pt, suggesting few arsenides and antimonides are present. There is, however, a good positive correlation between Pt and the IPGE (Figure 9c), indicating that these elements are concentrated in the same rocks and possibly by the same phase. The correlation between Pd and IPGE is not quite as good (Figure 9d), largely due to the low Pd contents in the UG1 chromitite.

In order to explain the correlation of the PGE with each other one might suggest that sulphides collected all the PGE. However, as mentioned above, in the UG-1 and UG-2 units the PGE do not correlate with S which suggests either that the collector phase was not sulphide or that S has been mobile in these units (Gain, 1985; Li *et al.*, 2004). The simplest model would be to suggest that the chromitites originally contained some disseminated sulphides which collected all the PGE from the magma. This sulphide was partially dissolved by late magmatic fluids (*e.g.* Gain, 1985), leaving behind the insoluble PGE and removing most of the S and, in the case of the UG-1, much of the Pd. Unfortunately we have no evidence for the original presence of the sulphide. Furthermore, if S and Pd-loss is the explanation for the lack of correlation between S and the PGE it still remains necessary to explain why the chromitite layers would originally have contained up to 10 times higher sulfide contents than the silicate rocks. One possibility is that the sulphides percolated down into the chromitites and were trapped there due to the high dihedral angles (Godel *et al.*, 2006). However, there is mostly a very sharp contrast in PGE content between the chromitites and their immediately adjacent silicate rocks (Figure 3), which requires that any vertical sulfide melt percolation would have been extremely efficient. One alternative is to appeal to laurite and isoferroplatinum crystallization for which there is equally little evidence**.**

Mantle-normalized multi element diagrams for most of our samples show the bell-shaped patterns characteristic of Upper Critical Zone rocks (Maier and Barnes, 1999) (Figure 10). Several features are worth highlighting:

i. The UG1 chromitite and its subsidiary stringers have strong negative Pd anomalies suggesting removal of Pd after sulfide accumulation.
ii. The UG1 pyroxenite has similar PGE patterns as the UG2 pyroxenite, lacking the negative Pd anomaly of the UG1 chromitites.
iii. Unlike most other Lower Zone and Critical Zone rocks, the UG2 pegmatoid has a distinct positive Pd anomaly suggesting selective late magmatic or post

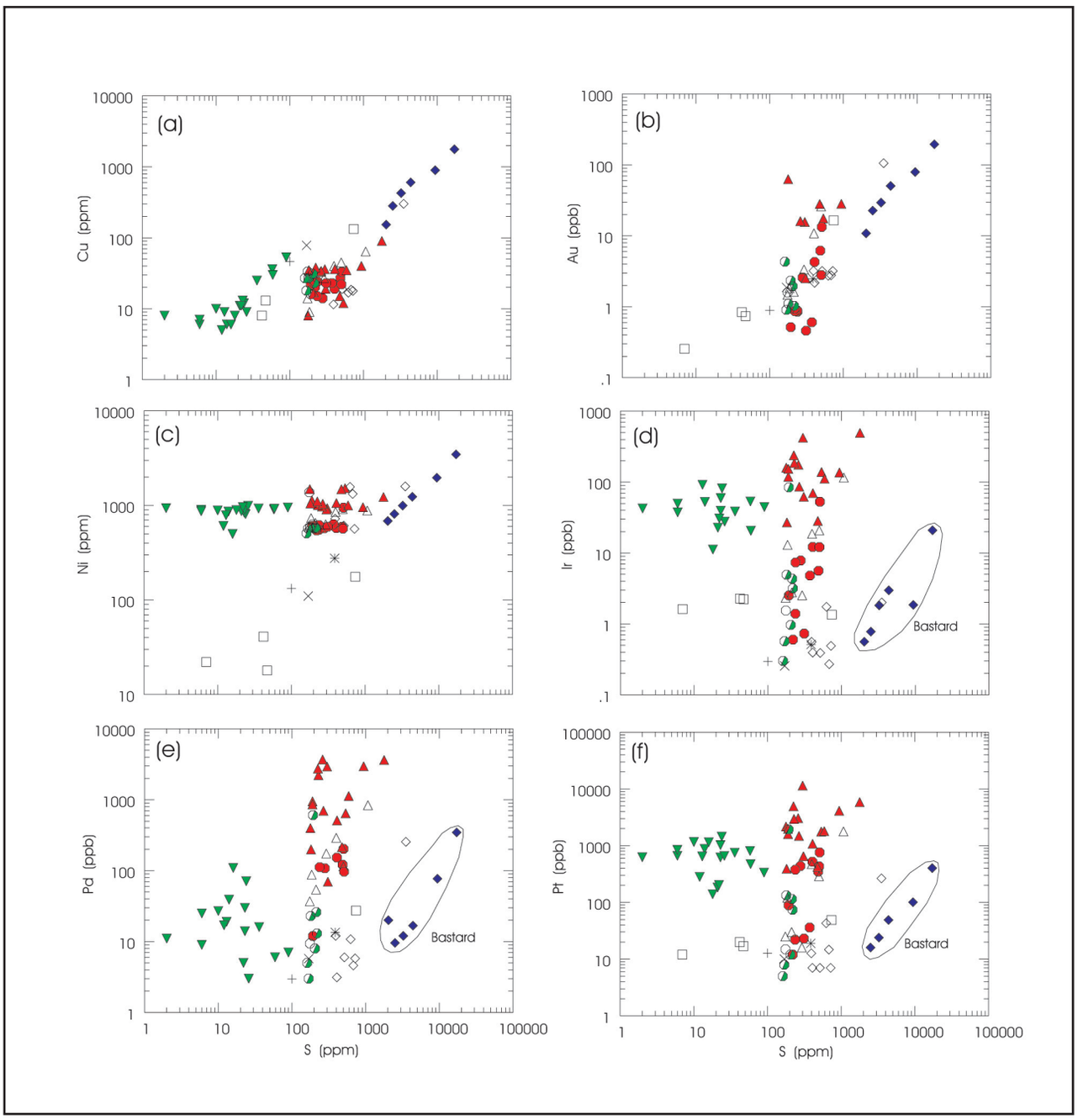

Figure 7. Binary variation diagrams vs S of (**a**) Cu, (**b**) Au, (**c**) Ni, (**d**) Ir, (**e**) Pd, (**f**) Pt. Data labels as in Figure 5.

magmatic addition of Pd. In contrast, Au shows little relative enrichment in the UG2 pegmatoid suggesting that it was less mobile than Pd.

PGE variation with height in the chromitite seams

In both the UG1 and UG2 chromitites, peak concentrations of the IPGE and Pt occur at the base and the top of the seams (Figure 11). An analogous PGE distribution has been observed elsewhere in the Bushveld (Figure 4). At some localities, *e.g.* at Marikana, where the UG2 is somewhat thicker than elsewhere in the Bushveld Complex the upper PGE peak is situated several dm below the upper contact of the seam. This has been interpreted as the result of merging between the less mineralized leader seams with the main seam (Davey, 1992). Incompatible lithophile elements such as Sm behave in a similar manner as the PGE, but Cr, Fe and V contents are highest in the centre of the seams.

The observed element distribution patterns are reminiscent of those in some dolerite sills interpreted to have resulted from flow differentiation (*e.g.* Coetzee *et al.*, 1995; Ross, 1986). Flow differentiation implies migration of suspended solid particles to the centre of a dyke- or sill-like magma body in response to grain dispersive forces acting on the flowing magma (Gibb, 1986). The enrichment of Cr, Fe and V in the centre of the chromitite seams reflects denser packing of chromite

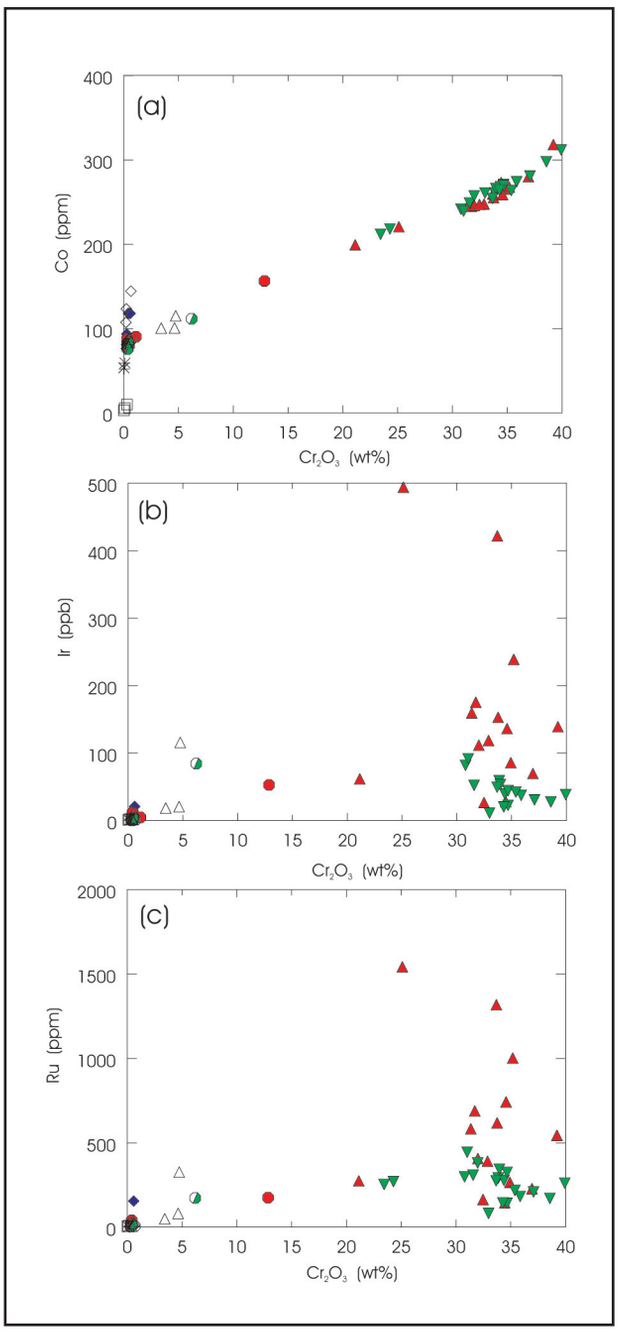

Figure 8. Binary variation diagrams of (**a**) Co vs Cr_2O_3, (**b**) Ir vs Cr_2O_3, and (**c**) Ru vs Cr_2O_3. Data labels as in Figure 5.

crystals, whereas the enrichment of incompatible elements at the margins may represent a higher liquid component. The similarity in the PGE and Sm distribution patterns could suggest that the PGE were also concentrated in a liquid, and the high concentrations of all PGE suggest that this liquid was a sulfide liquid. It needs to be modeled whether in slowly moving crystal slurries gravitative forces outweigh the grain dispersive forces resulting in high compaction rates at the base of the seams, but if our interpretation is correct the chromitites could have formed from a flowing crystal mush that was injected along broadly bedding-parallel fractures into semi-consolidated foot wall cumulates, along an inclined floor of the magma chamber. Analogous models have previously been suggested by Cameron (1978) and Lee (1981).

Mathez and Mey (2005) suggested that the chromitite seams may have acted as a barrier to ascending late magmatic fluids causing fluidization of the footwall cumulates. Fluidization may have aided downward injection of the chromitite into their footwall. Trapping of fluids below the chromitites is suggested by some of our data, notably the elevated Th/Sm ratios and Pd contents in the UG2 footwall pegmatoid. Such activity does however seem to be localized, as Cawthorn and Barry (1992) found no evidence for enrichment in incompatible and mobile elements in their samples of UG2 footwall pegmatoid.

A petrogenetic model for the formation of the chromitite and sulfide reefs of the Bushveld Complex

Many of the models that have been proposed to explain the formation of the chromitites and their PGE mineralization may be applicable to small intrusions, but it is difficult to imagine how gravitational fractionation, changes in oxygen fugacity, contamination, magma mixing, or emplacement of sulfide/chromite charged magma pulses could result in a broadly similar lithological and chemical stratigraphy across a 400 km wide intrusion. Pressure changes during magma chamber recharge represent an elegant alternative, but whether phase boundaries would shift significantly enough to be responsible for the accumulation of m-thick chromitite layers and the extremely well defined contacts between the chromitites and their host rocks remains to be modelled.

Here we propose an alternative mechanism for chromitite formation that could affect the entire intrusion, namely reconstitution of cumulates during down-dip sliding of semi-consolidated crystal mushes in response to late magmatic sagging of the centre of the intrusion. The process could be aided by building up of heat, released during cumulate solidification, beneath refractory chromitites and/or fluidization of footwall rocks beneath the relatively impermeable chromitites, although compositional evidence for the latter process, *e.g.* enrichment of mobile elements in the footwall rocks, is mostly lacking. Sagging or down faulting of igneous bodies during evacuation of magma chambers has long been documented in smaller magma systems where it resulted in the development of calderas (Williams and McBirney, 1979).

We suggest that prior to sagging, chromite largely occurred in disseminated form within its pyroxenitic or noritic host rocks. The spectacular layering between the chromitites and their anorthositic, pyroxenitic, and noritic hostrocks, often with knife sharp lithological contacts formed during down-dip sliding of chromite rich crystal slurries. We provide evidence for the process in the form of the symmetrical compositional zonation of

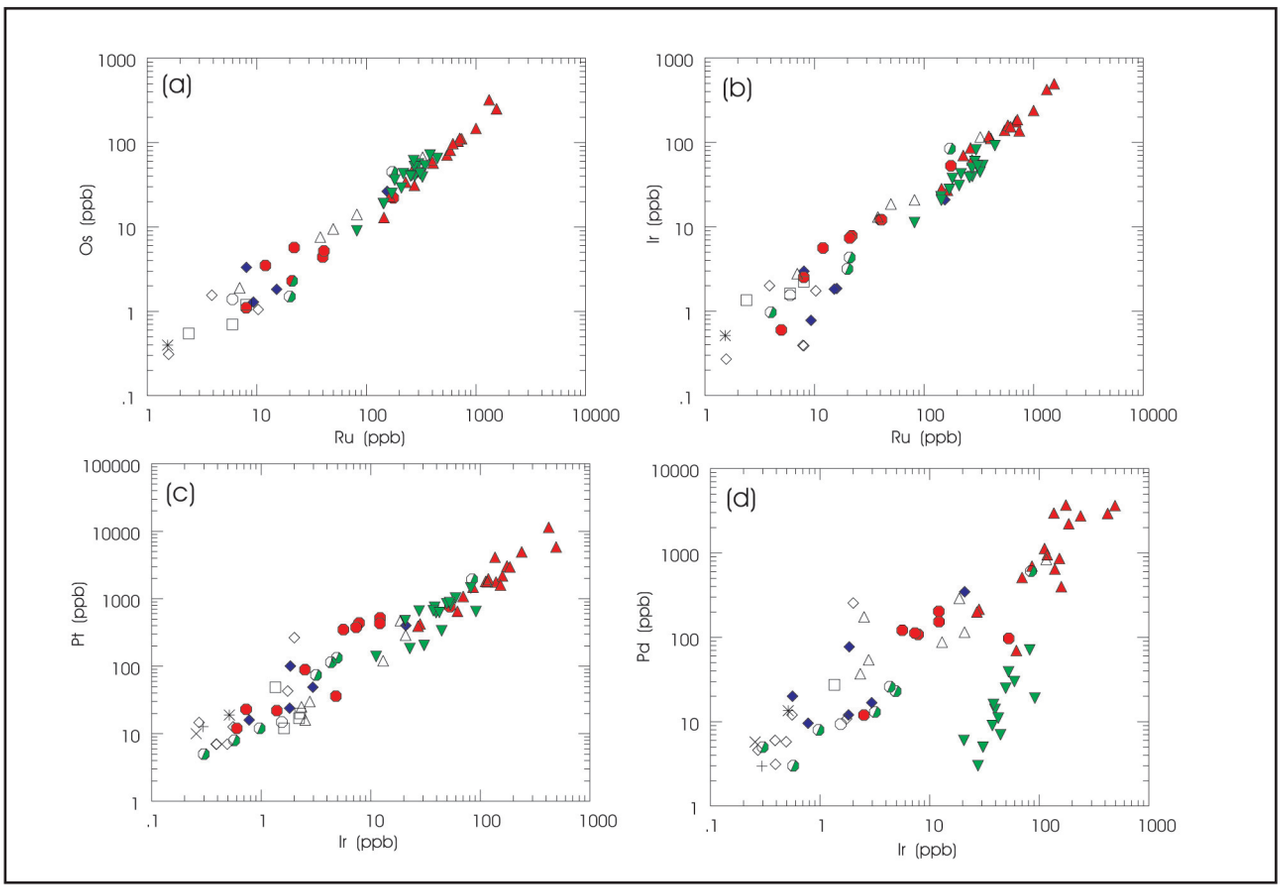

Figure 9. Binary variation diagrams of (**a**) Os vs Ru, (**b**) Irv s Ru, (**c**) Pt vs Ir, and (**d**) Pd vs Ir. Data labels as in Figure 5.

the chromitite layers (Figure 11). Examples of textures and structures resembling those in soft-sedimentological environments have previously been presented by Wadsworth (1973).

A key implication of our model is that the sulfide liquid that originally concentrated the PGE within the chromitites was also concentrated during cumulate sliding, and thus that chromitite-PGE reefs formed at a late magmatic stage. Chromite and sulfide liquid have similar densities, facilitating co-concentration during cumulate sagging and sliding. Furthermore, we propose that the formation of all Bushveld PGE reefs (*i.e.* including the sulfide reefs) is at least partly controlled by cumulate sagging and sliding, leading to concentration of sulfide liquid at the base of relatively permeable and melt enriched cumulate packages.

Other features that could be explained by cumulate sliding include:

i. Potholes (*e.g.* Carr *et al.*, 1994), particularly in the Upper Critical Zone where cumulate solidification was still incomplete by the time sagging occurred.
ii. The Boulder Bed, previously explained by the break-up of a pyroxenite layer during cumulate mobilisation (Jones, 1976).
iii. Localized upward intrusion of anorthosite into chromitite seams, as proposed by Nex (2004) for the UG1.
iv. Bifurcation and stacking of chromitite seams, locally resulting in composite packages consisting of main-, leader-, and footwall seams, and in compositional breaks within seams (*e.g.* UG2, Hiemstra, 1985).
v. Lateral thickness variations of individual sequences, *e.g.* the UG2-Merensky Reef interval in the western Bushveld Complex (Maier and Eales, 1997).
vi. "Beheaded" cyclic units (Eales *et al.*, 1988).

The model also provides an explanation for the occurrence of massive chromitites and high grade PGE reefs predominantly in large intrusions (Bushveld, Great Dyke, Stillwater). Comparison to the Molopo Farms intrusion in Botswana, assumed to be co-genetic to the Bushveld, is particularly instructive. The Molopo Farms Complex shows less pronounced layering than the Bushveld, it lacks thick chromitites and anorthosites, and PGE reefs are less metal-rich and less laterally continuous (von Gruenewaldt *et al.* 1989; Reichhardt, 1994). We suggest that this is due to the smaller size of the Molopo Farms intrusion (15.000 km^2 as opposed to 60.000 km^2 for the Bushveld), resulting in faster cooling and less pronounced late magmatic cumulate mobility.

A further important question relevant to exploration is whether the thickness and grade of PGE reefs systematically changes in the (primary magmatic) dip direction, as suggested *e.g.* in the Great Dyke (Wilson and Prendergast, 2001) and the Skaergaard intrusion

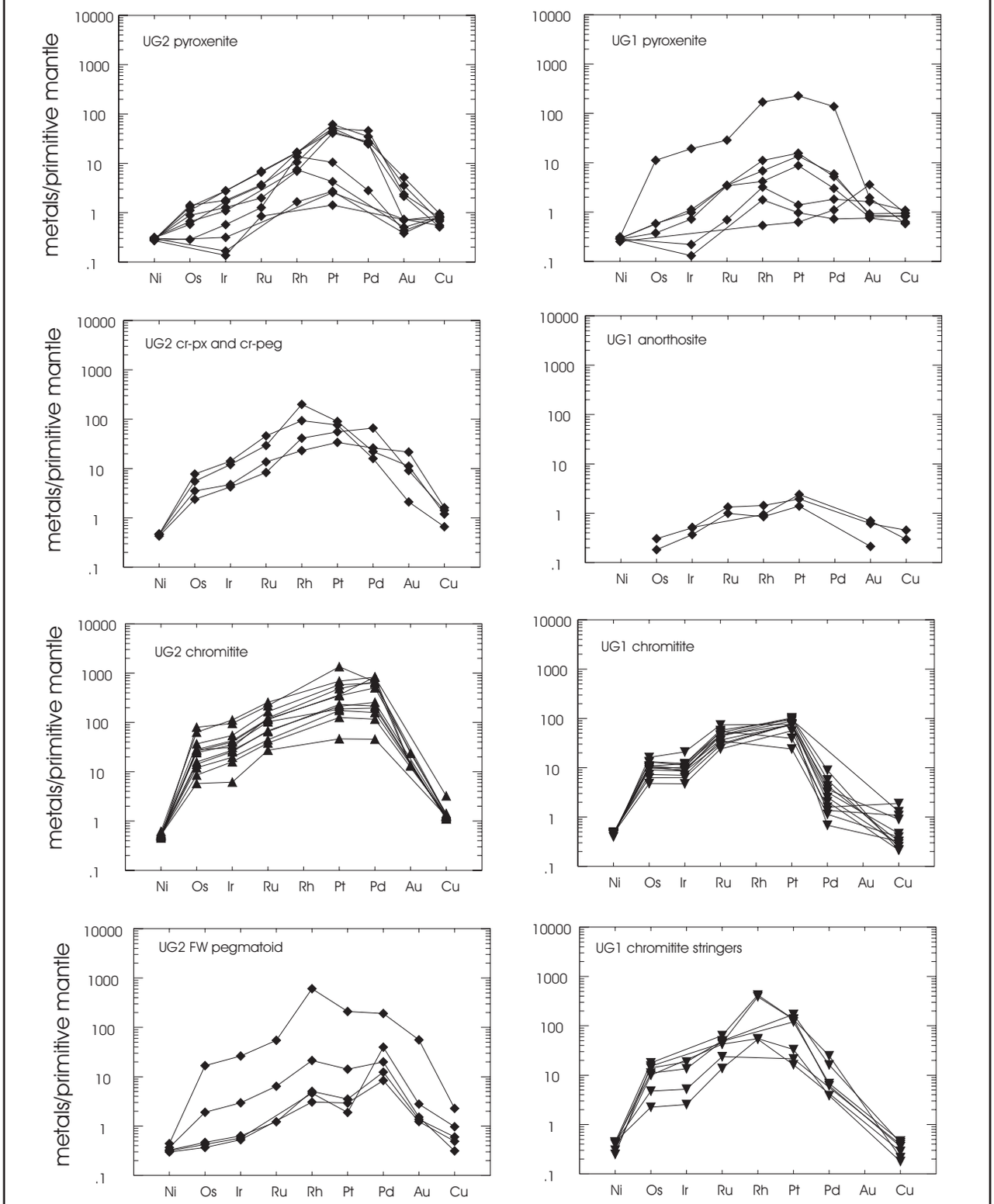

Figure 10. Multi-element diagrams of chalcophile elements for selected rocks. Normalization factors are from Barnes and Maier (1999).

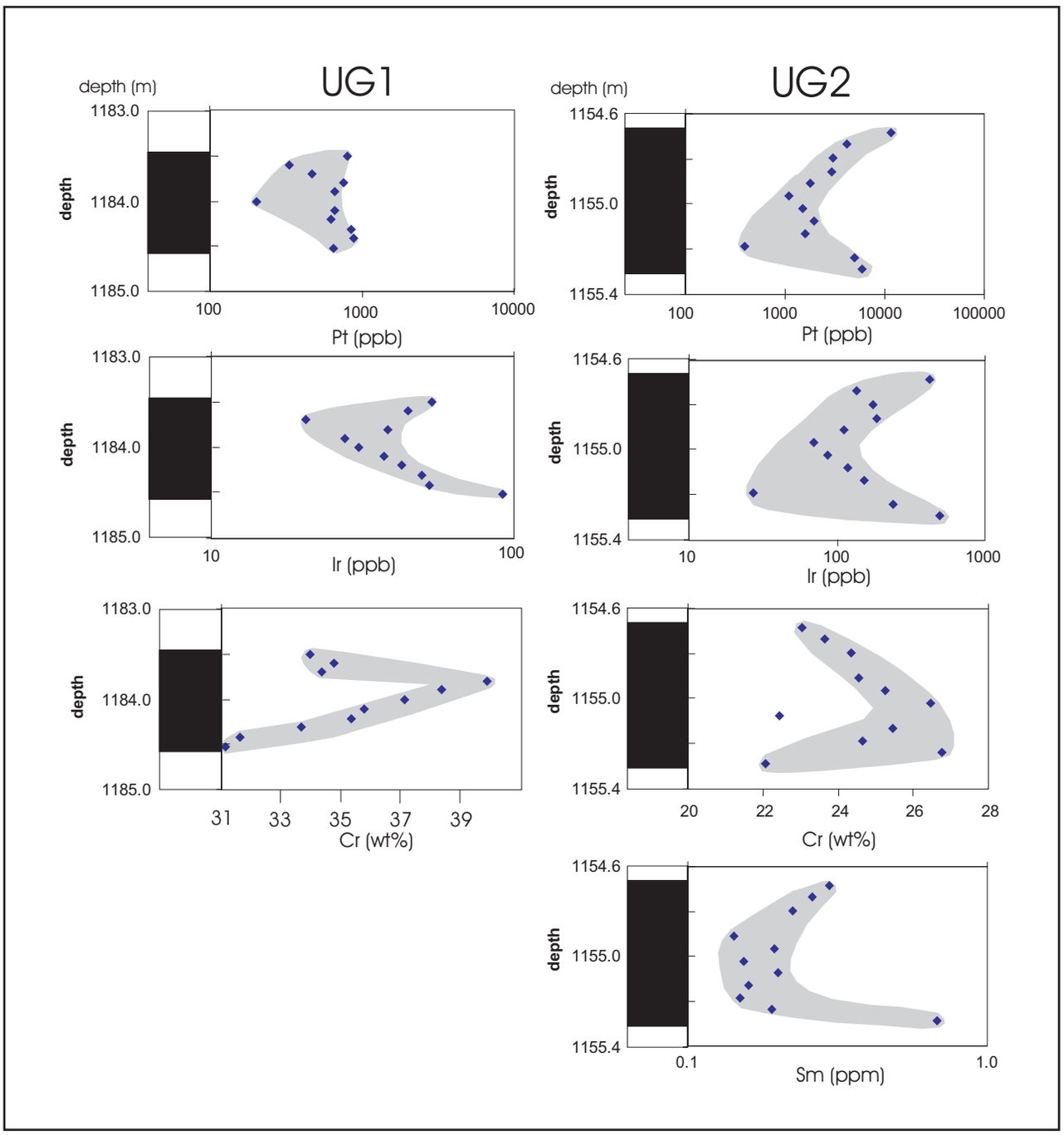

Figure 11. Distribution of selected elements through UG1 and UG2 chromitites. See text for discussion.

(Andersen *et al.*, 1998). Does the layering become more distinct or more diffuse in the down-dip direction, and do individual reefs become thinner and more PGE rich, or thicker and less PGE rich?

One of the last processes to affect the Bushveld PGE reefs comprised partial sulfide resorption by upward percolating late magmatic and/or hydrothermal melt/fluids during and after cumulate solidification (Gain 1985; Naldrett and Lehman 1988; von Gruenewaldt *et al.*, 1990). This led to localized Cu and Pd mobility and extremely high Pt/Pd ratios, *e.g.* in the UG1. Analogous to the processes discussed above, sulfide resorption was also more efficient in the Bushveld than in smaller, slowly cooling intrusions, explaining the relatively high Pt/Pd ratios and metal tenors of the Bushveld sulfides.

Acknowledgements

We thank Impala Platinum Ltd for providing the drillcore samples and for allowing publication of the results. SJB thanks NSERC for analytical funding. Steve Prevec and an anonymous reviewer provided helpful comments that led to a significant improvement of the manuscript.

References

Andersen J.C.O., Rasmussen H., Nielsen T.F.D., Ronsbo J.G. (1998) The Triple Group and the Platinova gold and palladium reefs in the Skaergaard

intrusion: stratigraphic and petrographic relations. *Economic Geology*, **93**, 488-509.

Barnes S-J and Maier W.D. (1999). The fractionation of Ni, Cu and the noble metals in silicate and sulphide liquids, *In:* R.R. Keays, C.M. Lesher, P.C. Lightfoot and C.E.G.Farrow (Editors). Dynamic processes in magmatic ore deposits and their application to mineral exploration: *Geological Association of Canada, Short Course Notes*, **13**, 69-106.

Barnes, S-J and Maier W.D. (2002a). Platinum-group elements and microstructures of normal Merensky Reef from Impala Platinum Mines, Bushveld Complex. *Journal of Petrology*, 43, 103-128.

Barnes, S-J and Maier W.D. (2002b). Platinum-group element distributions in the Rustenburg Layered Suite of the Bushveld Complex, South Africa. *In:* L.J. Cabri (Editor), The geology, geochemistry, mineralogy and mineral beneficiation of platinum-group elements. *Canadian Institute of Mining and Metallurgy Special Volume*, **54**, 431-458.

Bédard L.P. and Barnes S-J (2004). Improved Platinum-Group Element extraction by NiS Fire Assay from Chromitite Ore Samples Using a Flux Containing Sodium Metaphosphate. *Geostandards and Geoanalytical Research*, **28**, 311-316.

Bédard, L.P., Savard, D. and Barnes, S-J (2008) Total S concentration in geological reference materials by Elemental Infrared Analyser. *Geostandards and Geroanalytical Research*, **32**, 203-208.

Cameron E.N. (1978). The Lower Zone of the eastern Bushveld Complex in the Olifants River trough. *Journal of Petrology*, **19**, 437-462.

Cameron E.N. (1980). Evolution of the Lower Critical Zone, central sector, eastern Bushveld Complex and its chromite deposits. *Economic Geology*, **75**, 845-871.

Cameron E.N. and Desborough G.A. (1969). Occurrence and characteristics of chromite deposits – eastern Bushveld Complex. *Economic Geology Monograph*, **4**, 23-40.

Carr H.W., Groves D.I. and Cawthorn R.G. (1994) Controls on the distribution of Merensky Reef potholes at the Western Platinum mine, Bushveld Complex, South Africa: implications for disruptions of the layering and pothole formation in the Complex. *South African Journal of Geology*, **97**, 431-441.

Cawthorn R.G. (2005). Pressure fluctuations and the formation of the PGE-rich Merensky and chromitite reefs, Bushveld Complex. *Mineralium Deposita*, **40**, 231-235.

Cawthorn R.G. and Barry S.D. (1992). The role of intercumulus residua in the formation of pegmatoid associated with the UG2 chromitite, Bushveld Complex. *Australian Journal of Earth Science*, **39**, 263-276

Cawthorn R.G., Merkle R.K.W. and Viljoen M.J. (2002). Platinum-group element deposits in the Bushveld Complex, South Africa, *In:* L.J. Cabri (Editor). The geology, geochemistry, mineralogy and mineral beneficiation of platinum-group elements. *Canadian Institute of Mining and Metallurgy Special Volume*, **54**, 389-429.

Coertze F.J. and Schuman F.W. (1962). The basic portion and associated minerals of the Bushveld igneous Complex north of Pilanesberg. *Geological Survey of South Africa Bulletin*, **38**, 49p.

Coetzee M.S., Bate M.D. and Elsenbroek JH (1995). Flow differentiation – an explanation for the origin and distribution of plagioclase glomerocrysts in the Annas Rust dolerite sill, Vredefort Dome. *South African Journal of Geology*, **98**, 276-286.

Cousins C.A. and Feringa G, (1964). The chromite deposits of the western belt of the Bushveld Complex, 183-202. *In:* S. H. Haughton (Editor), The Geology of Some Ore Deposits in Southern Africa, *Geological Society of South Africa*, 730pp.

Curl, E.A. (2001). Parental magmas of the Bushveld Complex, South Africa. *Unpublished PhD Thesis, Monash University, Australia*, pp 140

Davey S.R. (1992). Lateral variations within the Upper Critical Zone of the Bushveld Complex on the farm Rooikoppies 297 JQ, Marikana, South Africa. *South African Journal of Geology*, **95**, 141-149.

De Bremond d'Ars J., Arndt N.T. and Hallot E. (2001). Analog experimental insights into the formation of magmatis sulfide deposits. *Earth and Planetary Science Letters*, **186**, 371-381.

Eales H.V. (2000). Implications of the chromium budget of the western limb of the Bushveld Complex. *South African Journal of Geology*, **103**, 141-150.

Eales H.V., Marsh J.S., Mitchell A.A., De Klerk W.J., Kruger F.J., and Field M. (1986). Some geochemical constraints upon models for the crystallization of the upper Critical Zone – Main Zone interval, northwestern Bushveld Complex. *Mineralogical Magazine*, **50**, 567-582.

Eales, H.V., Fields M., De Klerk W.F., Scoon R.N. (1988). Regional trends of chemical variation and thermal erosion in the Upper Critical Zone, Western Bushveld Complex, *Mineralogical Magazine*, **52**, 63-79.

Fourie G.P. (1959). The chromite deposits in the Rustenburg area: *Geological Survey of South Africa Bulletin*, **27**, 45pp.

Gain S.B. (1985). The geologic setting of the platiniferous UG2 chromitite layer on Maandagshoek, eastern Bushveld Complex. *Economic Geology*, **80**, 925-943.

Gibb F.G.F. (1986). Flow differentiation in xenolithic ultrabasic dykes of the Cuillins and the Strathaird Peninsula, Isle of Skye, Scotland. *Journal of Petrology*, **9**, 411-443.

Gingras P. (2002). Développement d'un processus analytique de préconcentration pour les éléments du groupe du platine et l'or. *Projet Fin d'Etude, Universite du Quebec Chicoutimi, Canada*, 42 pp.

Godel B., Barnes S-J, Maier W.D. (2006). Platinum-group elements in sulphide minerals, platinum-group minerals, and whole rocks of the Merensky Reef (Bushveld Complex, South Africa): implications for the formation of the reef. *Journal of Petrology*, **48**, 1569-1604.

Hatton C.J. and von Gruenewaldt G. (1987). The geological setting and petrogenesis of the Bushveld chromitite layers, *In:* C.W. Stowe (Editor). Evolution of Chromium Ore Fields. *Van Nostrand Reinhold, United States of America*, 109-143.

Hiemstra S.A. (1986). The distribution of chalcophile and platinum-group elements in the UG2 chromitite layer of the Bushveld Complex. *Economic Geology*, **81**, 1080-1086.

Irvine T.N. (1975). Crystallization sequences in the Muskox intrusion and other layered intrusions – II. Origin of chromitite layers and similar deposits of other magmatic ores. *Geochimica et. Cosmochimica. Acta*, **39**, 991-1020.

Irvine T.N. (1977). Origin of chromitite layers in the Muskox intrusion and other stratiform intrusions II: a new interpretation. *Geology*, **5**, 273-277.

Jackson E.D. (1961). Primary textures and mineral associations in the Ultramafic zone of the Stillwater Complex, Montana: *United States Geological Survey Professional Paper*, **358**, 106pp.

Jones J.P. (1976) Pegmatoidal nodules in the layered rocks of the Bafokeng leasehold area. *Transactions of the Geological Society of South Africa*, **79**, 312-320.

Kinnaird J.A., Kruger F.J., Nex P.A.M. and Cawthorn R.G. (2002). Chromite formation-a key to understanding processes of platinum enrichment. Transactions of the Institution of Mining and Metallurgy, **111**, B23-B35.

Kruger F.J. (2005). Filling the Bushveld magma chamber: lateral expansion, roof and floor interaction, magmatic unconformities, and the formation of giant chromitite, PGE and Ti-V magnetite deposits. *Mineralium Deposita*, **40**, 451-472.

Lee C.A. (1981). Post-depositional structures in the Bushveld Complex mafic sequence. *Journal of the Geological Society, London*, **138**, 327-341.

Lee C.A. (1983). Trace and latinum-group element geochemistry and the developmnt of the Merensky Unit of the western Bushveld Complex, *Minalium Deposita*, **8**, 173-190

Lee C.A. and Parry S.J. (1988). Platinum-group element geochemistry of the Lower and Middle Group chromitites of the eastern Bushveld Complex. *Economic Geology*, **83**, 1127-1139.

Leeb-du Toit A. (1986). The Impala Platinum Mines In: CR Anhaeusser and S Maske (Editors), Mineral Deposits of Southern Africa, *Geological Society of South Africa*, 1091-1106.

Li C, Ripley E.M., Merino E. and Maier W.D. (2004). Replacement of base metal sulfides by actinolite, epidote, calcite, and magnetite in the UG2 and Merensky Reef of the Bushveld Complex, South Africa. *Economic Geology*, **99**, 173-184.

Lipin B.R. (1993). Pressure increases, the formation of chromite seams, and the development of the Ultramafic series in the Stillwater Complex, Montana. *Journal of Petrology*, **34**, 955-976.

Maier W.D. (2005). Platinum-group element (PGE) deposits and occurrences: mineralization styles, genetic concepts, and exploration criteria. Invited presidential review, *Journal of African Earth Sciences*, **41**, 165-191.

Maier W.D. and Barnes S.-J. (1999). Platinum-group elements in silicate rocks of the lower, critical, and main zones at Union Section, western Bushveld Complex. *Journal of Petrology*, **40**, 1647-1671.

Maier W.D. and Barnes S.-J. (2003). Platinum-group elements in the Boulder Bed, western Bushveld Complex, South Africa. *Mineralium Deposita*, **38**, 370-380.

Maier W.D. and Eales H.V. (1997). Correlation within the UG2 - Merensky Reef interval of the Western Bushveld Complex, based on geochemical, mineralogical and petrological data. *Geological Survey South Africa Bulletin*, **120**, 56pp

Maier W.D., Prichard H.M., Barnes S.-J. and Fisher, P.C. (1999). Compositional variation of laurite at Union Section in the Western Bushveld Complex. *South African Journal of Geology*, **102**, 286-292.

Maier W.D. and Teigler B. (1995). A facies model for the Western Bushveld Complex. *Economic Geology*, **90**, 2343-2349.

Mathez E.A. and Mey J.L. (2005). Character of the UG2 chromitite and host rocks and petrogenesis of its pegmatoidal footwall, northeastern Bushveld Complex. *Economic Geology*, **100**, 1617-1630.

McLaren C.H. and De Villiers J.P.R. (1982). The platinum-group chemistry and mineralogy of the UG2 chromitite layer of the Bushveld Complex. *Economic Geology*, **77**, 1348-1366.

Merkle R.K.W. (1992). Platinum-group minerals in the middle group of chromitite layers at Marikana, western Bushveld Complex: indications for collection mechanisms and postmagmatic modification. *Canadian Journal of Earth Science*, **29**, 209-221.

Mondal S.K. and Mathez E.A. (2007). Origin of the UG2 chromitite layer, Bushveld Complex. *Journal of Petrology*, **48**, 495-510

Mossom R.J. (1986). The Atok Platinum Mine *In:* CR Anhaeusser and S Maske (Editors) Mineral Deposits of Southern Africa, *Geological Society of South Africa*, 1143-1154.

Naldrett, A.J., Lehmann, J. (1988). Spinel non-stoichiometry as the explanation for Ni-, Cu-, and PGE-enriched sulphides in chromitites. *In:* H.M. Pritchard, P.J. Pott, J.F.W. Bowles and S.J.Cribb (Editors). *Geo-Platinum 87. London, Elsevier Applied Science*, pp 113-143.

Naldrett A.J. and von Gruenewaldt G. (1989). Association of platinum-group elements with chromitite in layered intrusions and ophiolite complexes. *Economic Geology*, **84**, 180-187.

Nex, P.A.M. (2004). Formation of bifurcating chromitite layers of the UG1 in the Bushveld Igneous Complex, an analogy with sand volcanoes. *Journal of the Geological Society, London*, **161**, 903-909.

Nicholson D.M. and Mathez, E.A. (1991). Petrogenesis of the Merensky Reef in the Rustenburg section of the Bushveld Complex. *Contributions to Mineralogy and Petrology*, **107**, 293-309.

Potts, P.J., Gowing C.J.B. and Govindaraju K. (1992). Preparation, homogeneity evaluation and co-operative study of two new chomitite reference samples CHR-Pt+ and CHR-Bkg. *Geostandards Newsletter*, **16**, 81-108.

Potts, P.J., Tindle, A.G. and Webb, P.C. (1992). Geochemical reference material compositions. *Latherronwheel, Caithness, United Kingdom, Whittles Publishing, CRC Press, United Kingdom*.

Reichhardt, F.F. (1994). The Molopo Farms Complex, Botswana: history, stratigraphy, petrography, petrochemistry and Ni-Cu-PGE mineralization. *Exploration and Mining Geology*, **3**, 263-284.5-35.

Righter K, Campbell A.J., Humayun M. and Hervig R.L. (2004). Partitioning of Ru, Rh, Pd, Re, Ir, and Au between Cr-bearing spinel, olivine, pyroxene and silicate melts. *Geochimica et Cosmochimica Acta*, **68**, 867-880.

Ross M.E. (1986). Flow differentiation, phenocryst alignment, and compositional trends within a dolerite dyke at Rockport, Massachusetts. *Bullutin of the Geological Society of America*, **97**, 232-240.

Scoon R.J. and Teigler B. (1994). Platinum-group element mineralization in the Critical Zone of the Western Bushveld Complex: I sulfide-poor chromitites below the UG2. *Economic Geology*, **89**, 1094-1121

Sharpe M.R. (1981). The chronology of magma influxes to the eastern compartment of the Bushveld Complex, as exemplified by its marginal border group. *Journal of the Geological Society, London*, **138**, 307-326

Sharpe M.R. and Irvine T.N. (1983). Melting relations of two Bushveld chilled margin rocks and implications for the origin of chromitite. *Carnegie Institution of Washington Yearbook*, **82**, 295-300.

Snethlage R. and v Gruenewaldt G. (1977). Oxygen fugacity and its bearing on the origin of chromitite layers in the Bushveld Complex. In: D.D.Klemm and H.H. Schneider (Editors), Time and Stratabound Ore Deposits. *Springer Verlag, Berlin, Germany*, 352-370.

Steele T.W., Levin J., Copelowitz I. (1975). Preparation and certification of a reference sample of a precious metal ore. *South African Institute of Metallurgy Report*, **1696-1975**, 4p.

Teigler B. (1990a). Platinum-group element distribution in the Lower and Middle Group chromitites in the Western Bushveld Complex. *Mineralogy and Petrology*. **42**, 165-179.

Teigler B (1990b). Mineralogy, petrology and geochemistry of the lower and lower Critical Zones, northwestern Bushveld Complex. *Unpublished Ph.D. thesis, Rhodes University, Grahamstown, South Africa*, 247pp.

Teigler B. and Eales H.V. (1993). Correlation between chromite composition and PGE mineralization in the Critical Zone of the western Bushveld Complex. *Mineralium Deposita*, **28**, 291-302.

Ulmer G.C. (1969). Experimental investigation of chromite spinels. *Economic Geology Monograph*, **4**, 114-131

Von Gruenewaldt, G., Behr, S.H. and Wilhelm, H.J. (1989). Some preliminary petrological investigations of the Molopo Farms Complex, Botswana, and its Ni-Cu sulphide mineralization. *In:* M.D. Prendergast and M.J. Jones (Ediotrs). Magmatic Sulfides – the Zimbabwe Volume, *Institute of Mining and Metallurgy, London, England*, 95-105.

Von Gruenewaldt G, Dicks D., de Wet J. and Horsch H. (1990). PGE mineralization in the western sector of the eastern Bushveld Complex. *Mineralogy and Petrology*, **42**, 71-95

Von Gruenewaldt G. and Hatton, C.J. (1986). Geocongress 1986, Excursion 22A Guidebook, *Geological Society of South Africa*, 87pp.

Von Gruenewaldt G., Hatton C.J. and Merkle R.K.W., Gain S.B. (1986). Platinum-group element – chromitite associations in the Bushveld Complex. *Economic Geology*, **81,** 1067-1079

Von Gruenewaldt G. and Merkle R.K.W. (1995). Platinum-group element proportions in chromitites of the Bushveld Complex: implications for fractionation and magma mixing models. *Journal of African Earth Sciences*, **21**, 615-632.

Wadsworth W.J. (1973). Magmatic sediments. *Minerals, Science and Engineering*, **5**, 25-35.

Wager L.R. and Brown G.M. (1968). Layered igneous rocks. *Oliver and Boyd, Edinburgh and London, United Kingdom*, 588p.

Webb P.C., Thompson M., Potts P.J. and Bedard L.P. (2006). GEOPT18- An international proficiency test for analytical geochemistry laboratories - Report on round 18/Jan 2006 (Quartz diorite, KPT-1). *International Association of Geoanalysts*, 32pp, http://geoanalyst/org.

Williams H. and McBirney A.R. (1979). Volcanology. *Freeman, Cooper and Company, United States of America*, 397pp.

Wilson A.H. and Prendergast M.D. (2001). Platinum-group element mineralization in the Great Dyke, Zimbabwe, and its relationship to magma evolution and magma chamber structure. *South African Journal of Geology*, **104**, 319-342.

Editorial handling: H. Mouri